nature cell biology

Bcl-2 and accelerated DNA repair mediates resistance of hair follicle bulge stem cells to DNA-damage-induced cell death

Panagiota A. Sotiropoulou[1,3], Aurélie Candi[1,3], Guilhem Mascré[1], Sarah De Clercq[2], Khalil Kass Youssef [1], Gaelle Lapouge[1], Ellen Dahl[1], Claudio Semeraro[1], Geertrui Denecker[2], Jean-Christophe Marine[2] and Cédric Blanpain[1,4]

Adult stem cells (SCs) are at high risk of accumulating deleterious mutations because they reside and self-renew in adult tissues for extended periods. Little is known about how adult SCs sense and respond to DNA damage within their natural niche. Here, using mouse epidermis as a model, we define the functional consequences and the molecular mechanisms by which adult SCs respond to DNA damage. We show that multipotent hair-follicle-bulge SCs have two important mechanisms for increasing their resistance to DNA-damage-induced cell death: higher expression of the anti-apoptotic gene *Bcl-2* and transient stabilization of p53 after DNA damage in bulge SCs. The attenuated p53 activation is the consequence of a faster DNA repair activity, mediated by a higher non-homologous end joining (NHEJ) activity, induced by the key protein DNA-PK. Because NHEJ is an error-prone mechanism, this novel characteristic of adult SCs may have important implications in cancer development and ageing.

The maintenance and propagation of accurate genetic information is critical in ensuring the proper cellular function of all living organisms and in preventing cancer formation or ageing in mammals[1,2]. A great variety of DNA lesions, potentially modifying the genetic information, arise from assaults by the external environment. A highly conserved mechanism operates in all eukaryotic cells for recognizing DNA damage, alerting the cell to the damage, repairing the DNA lesions to maintain genome integrity and, if the damage is too extensive, stimulating cells to undergo either programmed cell death (apoptosis) or irreversible arrest of the cell cycle (senescence)[3–5]. Mutations in genes controlling any of these steps of the DNA damage response (DDR) have been associated with different human diseases such as accelerated ageing, neurodegenerative diseases and cancer[2,6].

Rupture of the sugar-phosphate DNA backbone, resulting in the formation of single-strand and double-strand breaks (DSBs) and thus leading to genetic instability, are among the most frequent DNA lesions[7]. Ionizing radiation (IR) produces multiple clusters of DSBs that are sensed by the multiprotein MRN (Mre11–Rad50–Nbs1) complex, which recruits and activates the ataxia telangiectasia mutated (ATM) kinase. Activation of ATM leads to the initiation of the DNA damage signal to the cell, resulting in the activation, stabilization and nuclear accumulation of p53 (ref. 8). Nuclear accumulation of p53 induces the transcriptional activation of different target genes that mediate cell-cycle arrest, apoptosis and DNA repair[9].

Most adult tissues, including the epidermis, the haematopoietic system and the intestine, undergo constant cellular turnover called tissue homeostasis[10]. SCs ensure tissue homeostasis by continuously providing new cells to replace the differentiated or damaged cells that are lost. Multipotent hair follicle (HF) SCs, residing in the specialized microenvironment called the bulge, ensure HF regeneration during homeostasis and epidermal repair after wounding[11]. Multipotent bulge SCs can be specifically isolated and functionally characterized within their native niche by using a combination of monoclonal antibodies including α-integrin and CD34 (refs 12–15). SCs are at high risk of accumulating deleterious mutations because they reside and self-renew in the adult tissues for extended periods. Little is known about how adult SCs sense DNA damage *in vivo* within their natural niche, how they activate DDR pathways, how they respond functionally to DNA damage, and how they repair DNA damage and ensure the propagation of accurate genetic information.

Here, using mouse epidermis as a model, we have determined the functional consequences and the underlying molecular mechanisms by which adult SCs respond to DNA damage in their native niche. We show that, after IR, bulge SCs are profoundly resistant to DNA-damage-induced apoptosis. The resistance of bulge SCs to apoptosis does not depend on relative quiescence and is not accompanied by their premature differentiation or cellular senescence. We show that

[1]Interdisciplinary Research Institute (IRIBHM), Université Libre de Bruxelles (ULB), 808, route de Lennik, BatC, C6-130, 1070 Brussels, Belgium. [2]VIB, UGent, Laboratory for Molecular Cancer Biology, Belgium.
[3]These authors contributed equally to this work.
[4]Correspondence should be addressed to C.B. (e-mail: Cedric.Blanpain@ulb.ac.be)

Received 29 March 2010; accepted 28 April 2010; published online 16 May 2010; DOI:10.1038/ncb2059

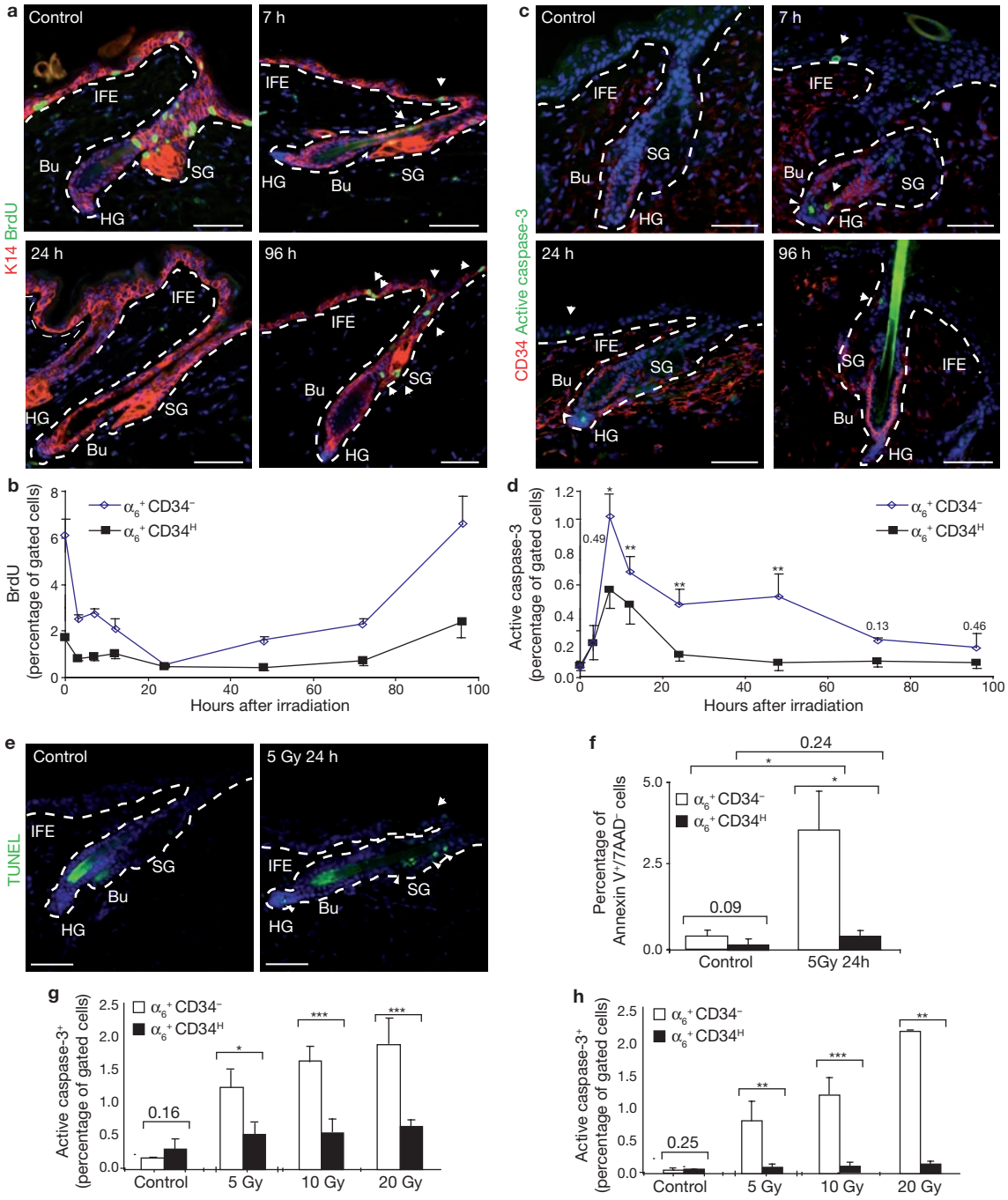

Figure 1 Bulge SCs are resistant to DNA-damage-induced cell death. (**a**) Kinetics of cell-cycle arrest following 5 Gy IR determined by immunofluorescence on skin sections of 7-week-old mice pulsed with BrdU for 4 h. Epidermal cells are marked with keratin 14 (K14). (**b**) Quantification of proliferation in bulge SCs (α_6^+ CD34^H) and in basal cells of the other compartments of skin epidermis (α_6^+ CD34$^-$) by FACS at the indicated time points after administration of 5 Gy IR in 7-week-old animals (error bars indicate s.e.m.; $n = 4$ mice; 20,000 bulge cells per mouse). (**c**) Apoptosis in 7-week-old mice as determined by active caspase-3 immunofluorescence at the indicated time points after 5 Gy IR. Bulge SCs are stained with anti-CD34 antibody. (**d**) Quantification of apoptosis by FACS using active caspase-3 at the indicated time points after 5 Gy IR (error bars indicate s.e.m.; $n = 8$ mice; 20,000 bulge cells per mouse). (**e**) Apoptosis as determined by TUNEL assay on skin sections, showing no apoptotic cells at 24 h after IR in bulge SCs. Arrowheads indicate apoptotic cells, all localized outside the bulge area. (**f**) Expression of early apoptotic marker (annexin V$^+$/7AAD$^-$) 24 h after 5 Gy IR in 7-week-old mice as determined by FACS analysis (error bars indicate s.e.m.; $n = 4$ mice; 20,000 bulge cells per mouse), showing that α_6^+ CD34$^-$ cells are still undergoing *de novo* apoptosis 24 h after IR. (**g**, **h**) Dose response to IR of basal epidermal cell apoptosis in 7-week-old mice as determined by FACS with active caspase-3 immnostaining 7 h (**g**) and 24 h (**h**) after IR (error bars indicate s.e.m.; $n = 3$ mice; 20,000 bulge cells per mouse). Scale bars, 50 μm. IFE, interfollicular epidermis; SG, sebaceous gland; Bu, bulge; HG, hair germ; asterisk, $P < 0.05$; two asterisks, $P < 0.01$; three asterisks, $P < 0.001$.

bulge SC resistance to DNA-damage-induced cell death is a consequence of higher expression of the anti-apoptotic protein Bcl-2 and the rapidly attenuated activation of p53, which is correlated with a faster DNA repair activity by NHEJ in bulge SCs.

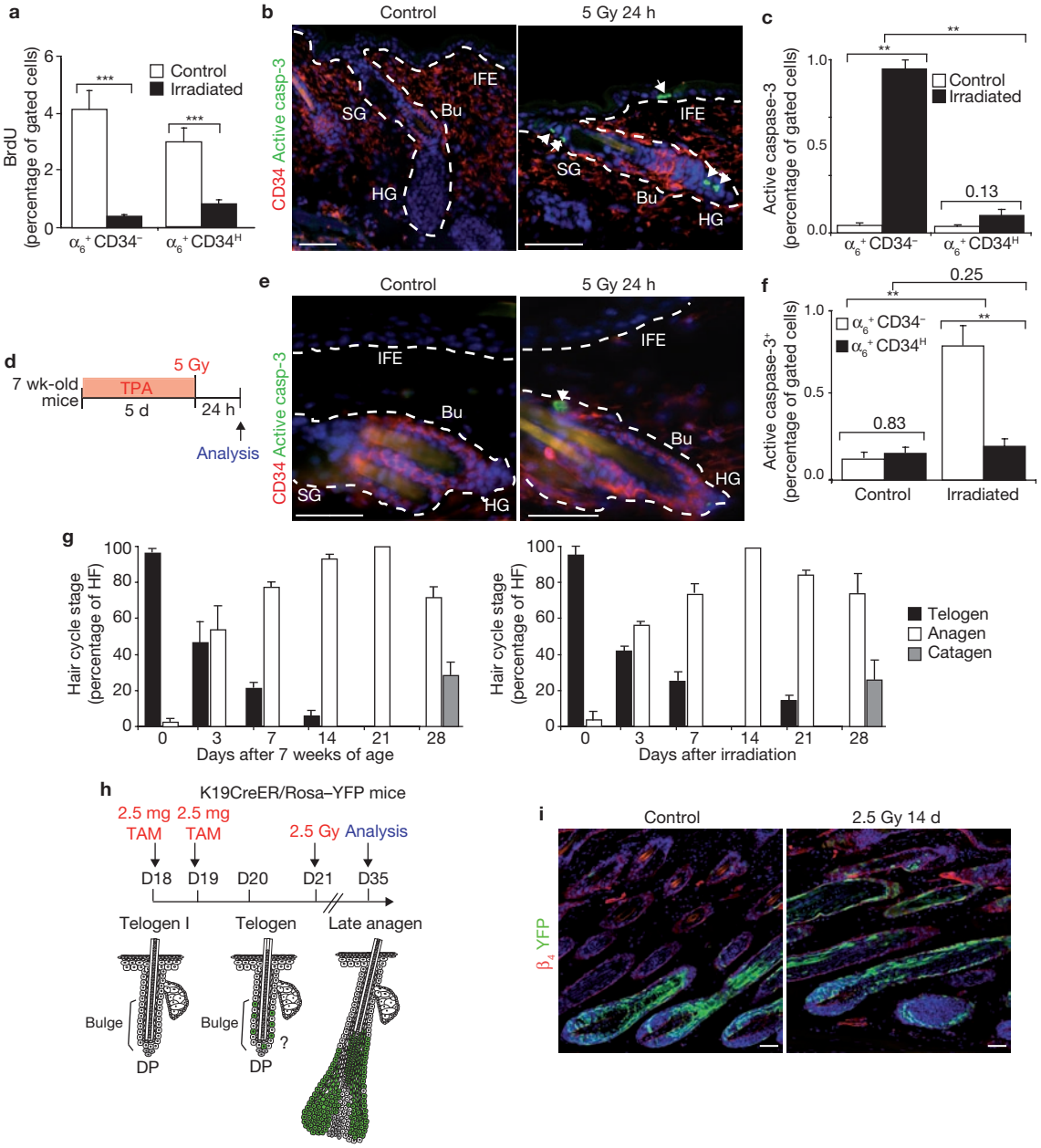

Figure 2 Resistance of bulge SCs to DNA-damage-induced cell death is not the result of their relative quiescence or the induction of senescence. (**a**) Quantification of proliferation in bulge SCs and the other basal cells in 23-day-old control mice and 24 h after 5 Gy IR (error bars indicate s.e.m.; $n = 12$ mice; 20,000 bulge cells per mouse). (**b**) Apoptosis after IR in 23-day-old mice as determined by immunofluorescence showing active caspase-3-positive cells (arrowheads) only outside the bulge SC population. (**c**) Quantification of apoptosis in bulge SCs and the other basal epidermal cells 24 h after 5 Gy IR in 23-day-old mice, by FACS analysis of active caspase-3 (error bars indicate s.e.m.; $n = 12$ mice; 20,000 bulge cells per mouse). (**d**) Scheme representing the protocol used to study apoptosis following DNA damage after exogenous induction of cell proliferation. Mice were treated with TPA for 5 days, subjected or not to 5 Gy IR and analysed 24 h later. (**e**) Apoptosis as determined by active caspase-3 immunofluorescence on skin sections of mice treated as indicated in **d**. (**f**) Quantification of apoptotic cells by FACS analysis of active caspase-3 in α_6^+ CD34^H and α_6^+ CD34$^-$ cells, in animals treated as indicated in **d**. Note the absence of apoptotic cells within the bulge SCs despite their increased cell proliferation (error bars indicate s.e.m., $n = 5$ mice; 20,000 bulge cells per mouse). (**g**) Quantification of the HFs in the different hair cycle stages in control and irradiated animals at the indicated time points after 5 Gy IR. No significant differences are observed between control and irradiated mice (error bars indicate s.e.m.; $n = 5$ mice; 100 follicular units per mouse). (**h**) Scheme showing the genetic lineage tracing approach used to follow the fate of bulge SCs 14 days after IR. D, day. (**i**) Analysis of the fate of genetically marked HF SCs in control mice and mice 14 days after IR, as illustrated in **h**. Scale bars, 50 μm. IFE, interfollicular epidermis; SG, sebaceous gland; Bu, bulge; HG, hair germ; asterisk, $P < 0.05$; two asterisks, $P < 0.01$; three asterisks, $P < 0.001$.

RESULTS

Resistance of bulge SCs to DNA-damage-induced cell death

To define the functional consequences of DNA damage for bulge SCs, we first assessed the consequences of IR to their proliferation and apoptosis. Administration of IR (5 Gy) to 7-week-old mice, when bulge SCs are mostly quiescent, induced a profound arrest of the cell cycle in all epidermal cells, including bulge SCs, lasting 96 h (Fig. 1a, b and Supplementary Information, Figs S1a and S2a). Early after IR, bulge SCs underwent apoptosis, although to

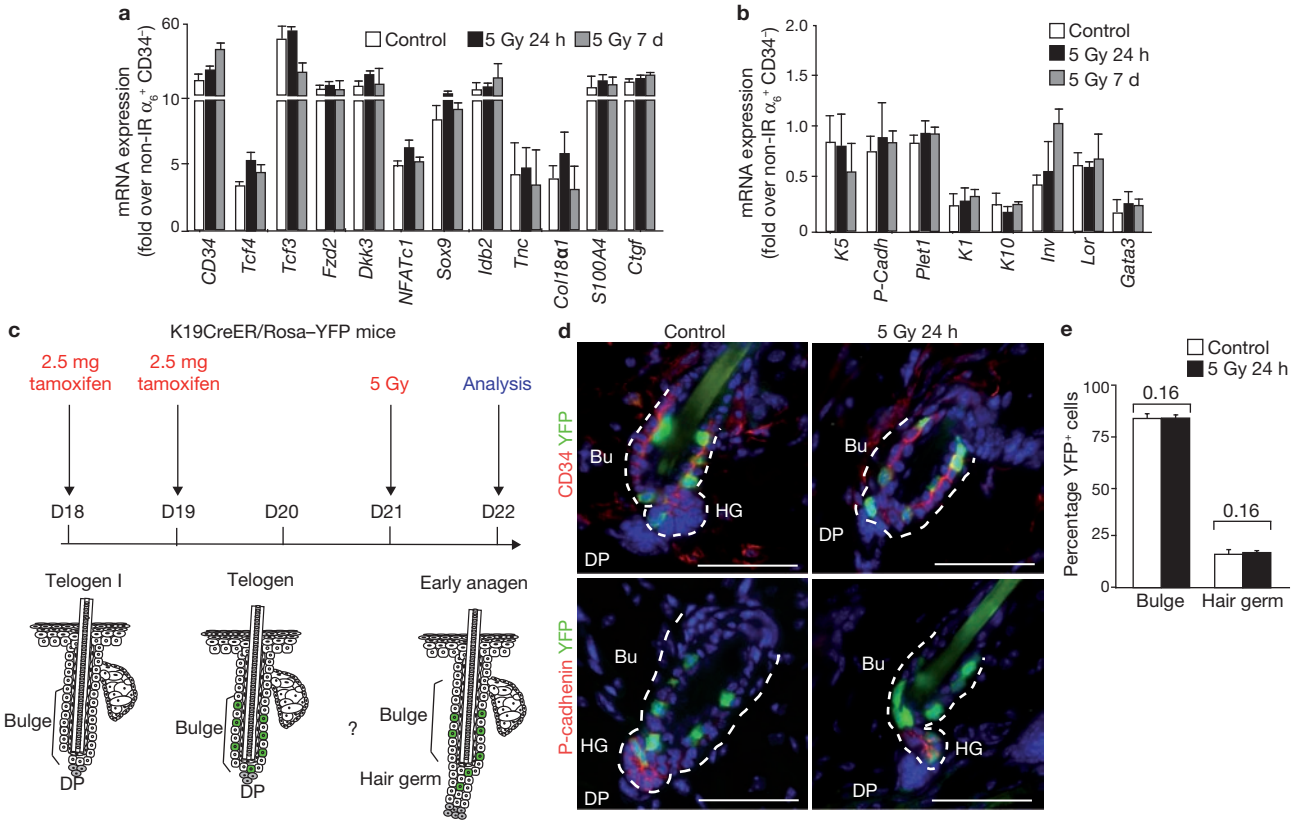

Figure 3 Bulge SCs retain their stemness and do not differentiate after DNA damage. (**a**, **b**) Quantitative RT–PCR analysis of mRNA expression of the main bulge markers (**a**) and keratinocyte differentiation-associated genes (**b**) in FACS-isolated cells from control mice and mice 24 h and 7 days after receiving 5 Gy IR (error bars indicate s.e.m.; $n = 3$ independent experiments). (**c**) Scheme representing the genetic targeting and the expected result of 24 h lineage tracing of bulge SCs, and the protocol used to induce and trace the fate of bulge SCs 24 h after IR. D, day. (**d**) Analysis of the expression of CD34 and P-cadherin in genetically marked HF SCs without IR or 24 h after administration of 5 Gy IR, as illustrated in **c**. (**e**) Quantification of YFP$^+$ cells within the bulge and the hair germ of control and irradiated mice, treated as presented in **c** (error bars indicate s.e.m.; $n = 4$ mice, 975 bulge cells per mouse); P values were estimated with Pearson's χ^2 test. Scale bars, 50 μm. IFE, interfollicular epidermis; SG, sebaceous gland; Bu, bulge; HG, hair germ; DP, dermal papillae; asterisk, $P < 0.05$; two asterisks, $P < 0.01$; three asterisks, $P < 0.001$.

a smaller extent than the other basal epidermal cells as measured by immunostaining for active caspase-3 (Fig. 1c, d and Supplementary Information, Figs S1b and S2b). However, 12 h after IR, apoptosis decreased sharply in bulge SCs, and it was no longer detectable after 24 h. In contrast, apoptosis reached the background level only 96 h after IR in the other basal epidermal cells (Fig. 1c, d and Supplementary Information, Fig. S1b). The enhanced survival of bulge SCs after IR was confirmed by TdT-mediated dUTP nick end labelling (TUNEL) assay (Fig. 1e). The presence of annexin V-positive/7AAD-negative cells (a hallmark of early apoptosis) in non-bulge epidermal cells 24 h after IR (Fig. 1f) indicates that the expression of late apoptosis markers (active caspase-3 and TUNEL) was not due to a decrease in the clearance of apoptotic bodies but rather to *de novo* apoptosis. Although the frequency of apoptosis increased with the dose of IR in non-bulge cells, there was no further increase in apoptosis in bulge SCs 7 and 24 h after IR (Fig. 1g, h). To explore the role of the genetic background in the sensitivity of keratinocytes to DNA-damage-induced cell death, we used different mouse strains showing different radiosensitivity of thymocytes[16]. Although we observed some difference in the frequency of apoptosis in non-bulge cells, there was no significant difference between the mouse strains in the level of apoptosis in bulge SCs 7 and 24 h after IR (Supplementary Information, Fig. S3a), indicating that genetic background does not influence the resistance of bulge SCs to apoptosis after IR.

Resistance of bulge SCs to apoptosis is not the result of their relative quiescence, the induction of senescence or their premature differentiation

One possible explanation for the resistance of bulge SCs to DNA-damage-induced cell death is their greater quiescence during the resting stage of the hair cycle, because apoptotic sensitivity to IR has been correlated with cell proliferation[17]. We therefore investigated the outcome of IR during the activation and proliferation of bulge SCs that accompany HF regeneration[18] (Fig. 2a and Supplementary Information, Fig. S3b, c). During their proliferation stage, bulge SCs underwent cell-cycle arrest in a similar manner to that of the other basal epidermal cells (Fig. 2a), but they were still profoundly resistant to DNA-damage-induced apoptosis (Fig. 2b, c and Supplementary Information, Fig. S3d). Stimulating the proliferation of bulge SCs by 5 days of treatment with 12-*O*-tetradecanoylphorbol-13-acetate (TPA) before administration of IR did not inhibit the resistance of bulge SCs to apoptosis (Fig. 2d–f), indicating that resistance of bulge SCs to DNA-damage-induced cell death is not related to their relative quiescence.

Another possibility is that bulge SCs do not undergo apoptosis, so as to preserve the architecture of epidermis temporarily, but instead undergo cellular senescence[8]. After IR, bulge SCs did not show increased expression of senescence-associated β-galactosidase activity (Supplementary

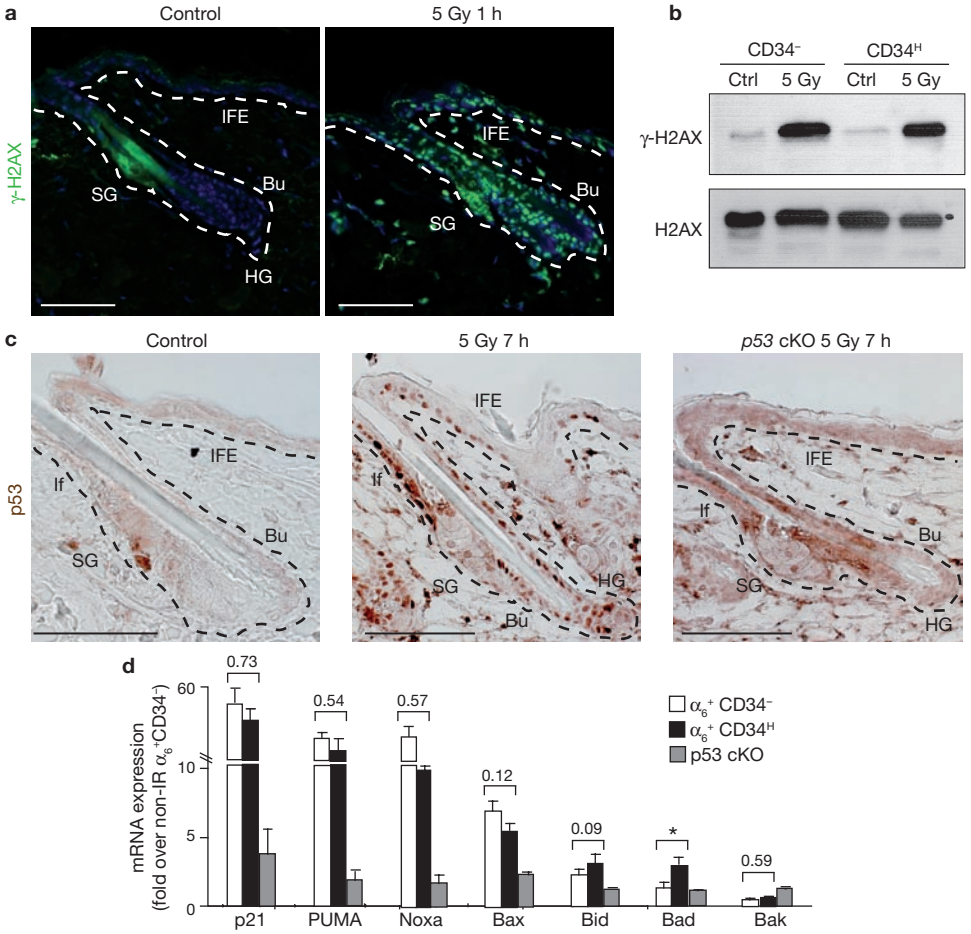

Figure 4 Bulge SCs undergo DNA damage after IR and activate the DDR pathway. (**a**) DSB detection using γ-H2AX immunostaining before and after IR. (**b**) Western blot analysis of H2AX and γ-H2AX in $CD34^-$ and $CD34^H$ populations. Ctrl, control. (**c**) Immunohistochemistry for p53 expression of control and irradiated mice. Skin sections of *p53* conditional knockout (cKO) mice in the epidermis were used as negative control for the staining (right panel). (**d**) Expression of the canonical p53 target genes in 7-week-old mice after IR, as evaluated by quantitative RT–PCR analysis of FACS-isolated cells of wild-type and *p53* cKO mice in the epidermis. Results are presented as fold change from the non-irradiated α_6^+ $CD34^-$ population (error bars indicate s.e.m.; $n = 5$ independent experiments). Scale bars, 50 μm. IFE, interfollicular epidermis; SG, sebaceous gland; Bu, bulge; HG, hair germ; DP, dermal papillae; asterisk, $P < 0.05$; two asterisks, $P < 0.01$; three asterisks, $P < 0.001$.

Information, Fig. S4a). Bulge SC-mediated HF regeneration was also not compromised by IR, as shown by the normal increase in the percentage of HF in their growth stage in the weeks after IR administration (Fig. 2g–i and Supplementary Information, Fig. S4b). When epidermal cells were activated to proliferate by treatment with TPA, bulge SCs of control and irradiated mice incorporated bromodeoxyuridine (BrdU) in a similar manner (Supplementary Information, Fig. S4c–f), demonstrating that acute administration of IR does not impair the ability of bulge SCs to proliferate in response to mitogenic signals. Administration of repeated doses of IR during 3 or 10 consecutive weeks did not result in a decrease in bulge SCs or in their ability to proliferate naturally or after administration of TPA (Supplementary Information, Fig. S4g–o). As a consequence of the transient cell-cycle arrest, single or repeated doses of IR resulted in a mild desynchronization of HF cycling, transiently increasing the proportion of HF in telogen (Fig. 2g and Supplementary Information, Fig. S4p). Taken together, these results indicate that bulge SCs do not undergo cellular senescence after DNA damage.

It has been recently demonstrated that melanocyte SCs, which share the same niche with bulge SCs, undergo premature differentiation on DNA damage[19]. To determine whether IR induced the differentiation of bulge SCs, we used RT–PCR of fluorescence-activated cell sorting (FACS)-isolated cells and immunostaining (Fig. 3a, b and Supplementary Information, Figs S2c–e and S5), the expression after IR of a panel of well characterized bulge-specific and epidermal differentiation markers specific for cell lineages into which bulge SCs can differentiate. We did not observe any difference in the expression of bulge-specific or differentiation markers in bulge SCs at 24 h and 1 week after IR (Fig. 3a, b and Supplementary Information, Fig. S5), suggesting that IR did not induce rapid differentiation of bulge SCs and that the intrinsic properties of tissue-specific SCs are more important than the surrounding environment in controlling the functional response of SCs to DNA damage.

Another possible explanation for the observed resistance of bulge SCs to DNA-damage-induced apoptosis would be that, after IR, they lose CD34 expression and migrate out of their niche. To exclude this possibility we performed genetic lineage-tracing experiments of bulge SCs[20] and followed their fate and localization 24 h after IR (Fig. 3c). By quantifying the localization (bulge or germ) of yellow fluorescent protein (YFP)-tagged cells, we did not find any significant difference between irradiated and control mice (Fig. 3d, e), strongly suggesting that bulge SCs do not rapidly lose CD34 expression or migrate out of their niche on DNA damage.

DNA damage induces p53 stabilization and upregulation of canonical target genes of p53 in bulge SCs

To identify the molecular mechanism underlying the resistance of bulge SCs to apoptosis, we investigated at which step of the DDR, from the initial sensing of DNA lesions to the activation of p53, the differences between bulge SCs and other epidermal cells arise. At 1 h after DNA damage, H2AX phosphorylation occurred similarly in bulge SCs and the other cells of epidermis (Fig. 4a, b), indicating that detection of DNA damage and activation of the early steps of the DDR transduction machinery occur normally in bulge SCs and that the bulge niche microenvironment does not protect SCs from undergoing DNA damage.

Activation of the DDR pathway leads to the stabilization of p53 and to the induction of p53-regulated transcriptional target genes[9], which is required for DNA-damage-induced cell-cycle arrest and apoptosis in the epidermis, as well as alopecia after DNA damage, because these responses are not observed in *p53*-null mice[21,22] or after conditional deletion of *p53* in the epidermis (Supplementary Information, Fig. S6). At 7 h after IR, p53 was detectable in most basal cells of the epidermis including bulge SCs (Fig. 4c), indicating that under normal circumstances p53 is initially stabilized in bulge SCs. We next tested whether a difference in the transcriptional program of *p53* could account for the resistance of bulge SCs to DNA damage. Using quantitative RT–PCR, we compared the levels of expression of p53 target genes in FACS-isolated cells at 7 h after IR. The best characterized pro-apoptotic p53 target genes such as *Puma*, *Noxa* and *Bax*[23] were upregulated in both bulge and non-bulge cells, indicating that the survival of bulge SCs is not due to their inability to upregulate the expression of pro-apoptotic p53 target genes (Fig. 4d).

Higher expression of Bcl-2 contributes to increased resistance to DNA-damage-induced cell death in bulge SCs

The execution of caspase-mediated apoptosis relies on the interaction between pro-apoptotic (such as *Bax* and *Bak*) and anti-apoptotic (such as *Bcl-2*, *Mcl-1* and *Bcl-X$_L$*) members of the *Bcl-2* family[24]. Interestingly, levels of *Bcl-2* mRNA and Bcl-2 protein are significantly higher in bulge SCs than in other epidermal cells[25] (Fig. 5a, b). We therefore investigated the functional consequence of IR in *Bcl-2*-deficient mice[26]. An absence of Bcl-2 resulted in a marked, proportionally greater increase in DNA-damage-induced apoptosis in bulge SCs (Fig. 5c, d), indicating that higher basal Bcl-2 levels are at least partly responsible for the resistance of the bulge SCs to DNA-damage-induced apoptosis.

Rapid inhibition of p53 activity promotes bulge SC survival after DNA damage

The rapid decline in apoptosis of bulge SCs after IR suggests that other factors besides Bcl-2 are likely to be involved in the higher resistance of bulge SCs. One possibility could be a more transient p53 activation in bulge SCs after IR. We therefore investigated the spatio-temporal expression of p53 in epidermis after IR. Expression of p53 was rapidly downregulated after DNA damage in bulge SCs and was barely detectable after 24 h, whereas the protein was still expressed in the other epidermal cells (Fig. 6a–c). To determine whether the more transient expression of p53 in bulge SCs could account for their resistance to apoptosis, we used *Mdm2* mouse mutants[27] to increase the strength and length of p53 expression. *Mdm2*$^{puro/-}$ mice express low levels of Mdm2 and show sustained p53 expression after IR[27]. Irradiation of *Mdm2*$^{puro/-}$ mice resulted in sustained expression of p53 and a marked increase in apoptosis in bulge SCs 24 h after IR (Fig. 6d–g).

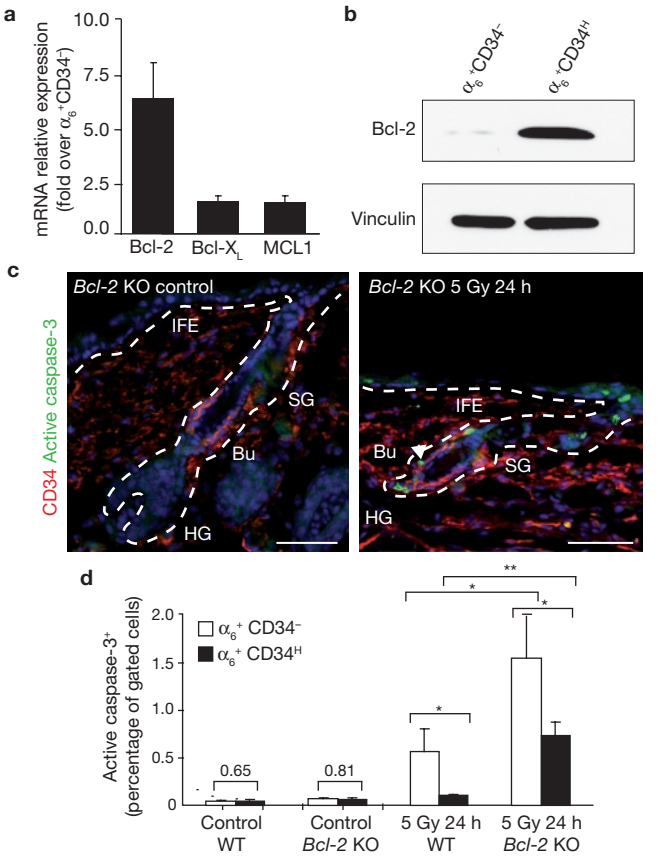

Figure 5 Higher Bcl-2 expression protects bulge SCs from DNA-damage-induced apoptosis. (**a**) Quantitative RT–PCR analysis of mRNA expression of the main anti-apoptotic genes in FACS-isolated cells (error bars indicate s.e.m.; $n = 4$ independent experiments). (**b**) Western blot analysis of Bcl-2 expression performed on FACS-isolated cells. Uncropped images of blots are shown in Supplementary Information, Fig. S8a. (**c**) Apoptosis after IR in 23-day-old *Bcl-2* knockout (*Bcl-2* KO) mice. The arrowhead indicates an active caspase-3-positive bulge SC. (**d**) Quantification of active caspase-3-positive cells by FACS in wild-type (WT) and *Bcl-2* KO mice without IR or 24 h after IR (error bars indicate s.e.m.; $n = 8$ mice; 20,000 bulge cells per mouse). Scale bars, 50 μm. IFE, interfollicular epidermis; SG, sebaceous gland; Bu, bulge; HG, hair germ; If, infundibulum; asterisk, $P < 0.05$; two asterisks, $P < 0.01$; three asterisks, $P < 0.001$.

These data indicate that the rapid downregulation of p53 contributes to the resistance of bulge SCs to DNA-damage-induced cell death.

The more rapid clearance of p53 in bulge SCs is not caused by a greater increase in Mdm2 expression after IR. On the contrary, the level of Mdm2 was lower in bulge SCs 24 h after IR (Fig. 6c), which is consistent with the accelerated p53 degradation, and the fact that Mdm2 expression is under the control of p53 in a negative feedback loop[28].

Higher DNA-PK-mediated NHEJ activity accelerates DNA repair and protects bulge SCs from undergoing apoptosis

The transient phosphorylation of p53 at Ser 15 in bulge SCs (Fig. 6c), a hallmark of DNA damage[29], indicates that the more rapid downregulation of p53 could result from a more rapid disappearance of DNA lesions. To test this possibility, we assessed the expression of γ-H2AX, which correlates with the persistence of unrepaired DSBs[30], at different time points after IR by immunofluorescence on skin sections and on Cytospin slides of FACS-isolated cells (Fig. 7a, b and Supplementary Information,

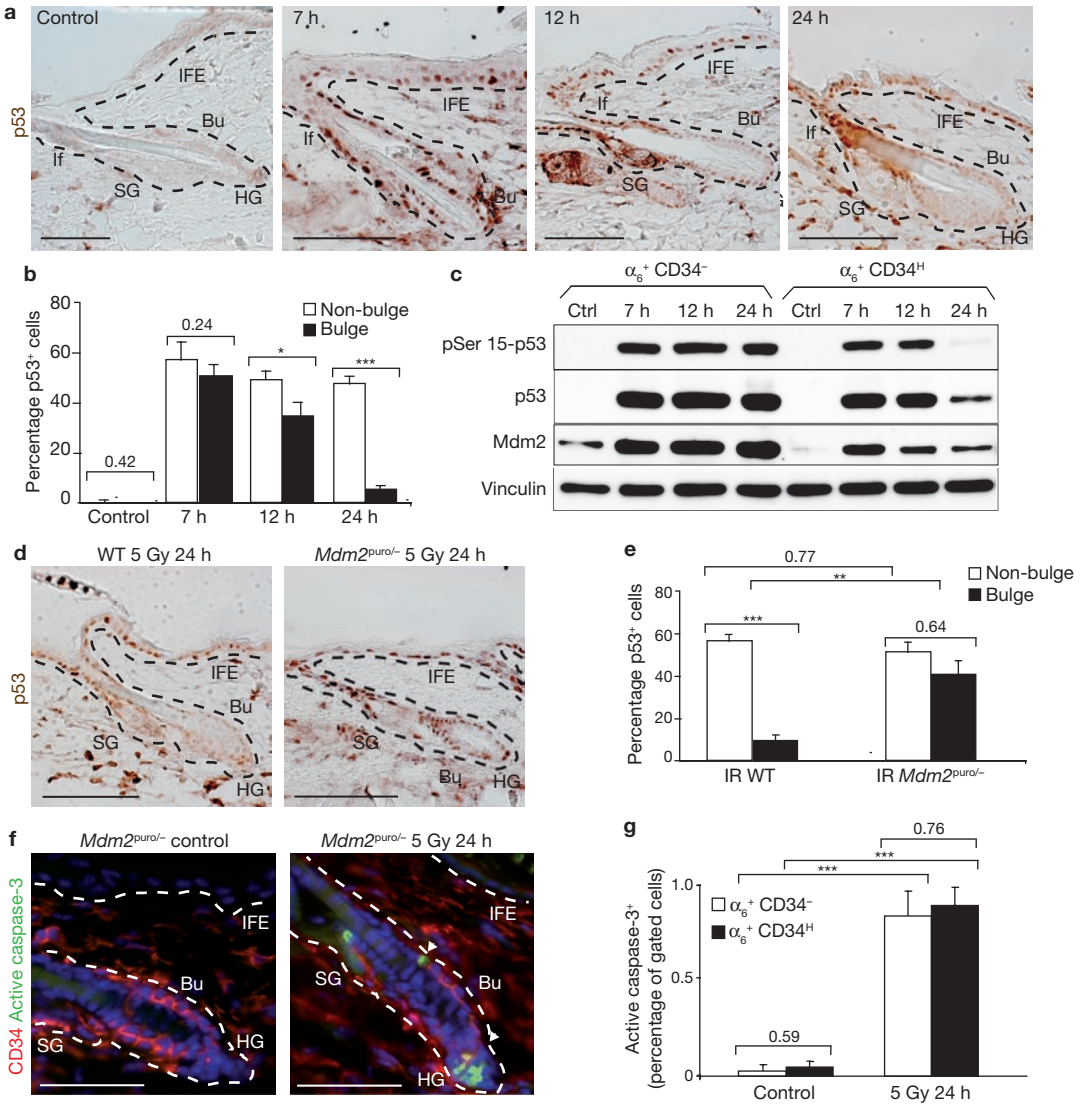

Figure 6 Transient p53 expression protects bulge SCs from DNA-damage-induced apoptosis. (**a**) Temporal analysis of p53 expression after IR by immunohistochemistry. Note the more rapid clearance of p53 in the bulge area. (**b**) Quantification of p53-positive cells within the bulge area and other epidermal cells per HF unit (interfollicular epidermis, hair germ and infundibulum) on the immunohistochemistry images (error bars indicate s.e.m.; $n = 4$ mice, 60 follicular units per mouse). Ctrl, control. (**c**) Temporal western blot analysis of expression of Mdm2, p53 and p53 phosphorylated at Ser 15 (pSer 15-p53) after IR in FACS-isolated cells, showing the faster downregulation of p53 and pSer 15-p53 in bulge SCs, without a concomitant increase in Mdm2 expression. Vinculin was used as a loading control. Uncropped images of blots are shown in Supplementary Information, Fig. S8b. (**d**, **e**) Immunohistochemistry of p53 expression (**d**) and the relative quantification of p53-positive cells (**e**) in wild-type (WT) and *Mdm2*$^{puro/-}$ mice 24 h after 5 Gy IR (error bars indicate s.e.m.; $n = 4$ mice, 60 follicular units per mouse). (**f**) Analysis of apoptosis in control and irradiated *Mdm2*$^{puro/-}$ mice by active caspase-3 immunofluorescence. Arrowheads indicate apoptotic cells. (**g**) Quantification of apoptotic cells without IR and 24 h after 5 Gy IR in *Mdm2*$^{puro/-}$ mice (error bars indicate s.e.m.; $n = 3$ mice; 20,000 bulge cells per mouse). Scale bars, 50 μm. IFE, interfollicular epidermis; SG, sebaceous gland; Bu, bulge; HG, hair germ; If, infundibulum; asterisk, $P < 0.05$; two asterisks, $P < 0.01$; three asterisks, $P < 0.001$.

Fig. S7a). These assays showed that γ-H2AX foci disappear more rapidly in bulge SCs after IR than in other epidermal cells. Another early event during DDR is the clustering of 53BP1 at the site of DNA damage[31]. We found that at 7 h after IR the 53BP1 nuclear foci were more abundant in the other basal epidermal cells than in bulge SCs (Fig. 7c and Supplementary Information, Fig. S7b, c). Quantification of DNA damage using comet assay on FACS-isolated cells showed that bulge SCs showed an increase in cells without any sign of DNA damage concomitantly with a decrease in cells with severe DNA lesions (stages 4/5) at 7 and 24 h after IR (Fig. 7d and Supplementary Information, Fig. S7d, e). Taken together, these data indicate that DNA repair is more rapid in bulge SCs than in other epidermal cells.

The majority of DSBs in cells that are in the G0/G1 stage of the cell cycle are repaired by NHEJ[32]. Because most epidermal cells are in the G0/G1 stage[13,15], we examined whether the accelerated DNA repair activity of bulge SCs is mediated by a greater NHEJ activity. Using an *ex vivo* assay that measures the repair of a green fluorescent protein (GFP) reporter construct cleaved by a restriction enzyme, we showed that, whereas bulge and non-bulge cells are electroporated with the same efficiency, as demonstrated by the similar expression of uncleaved tdTomato plasmid

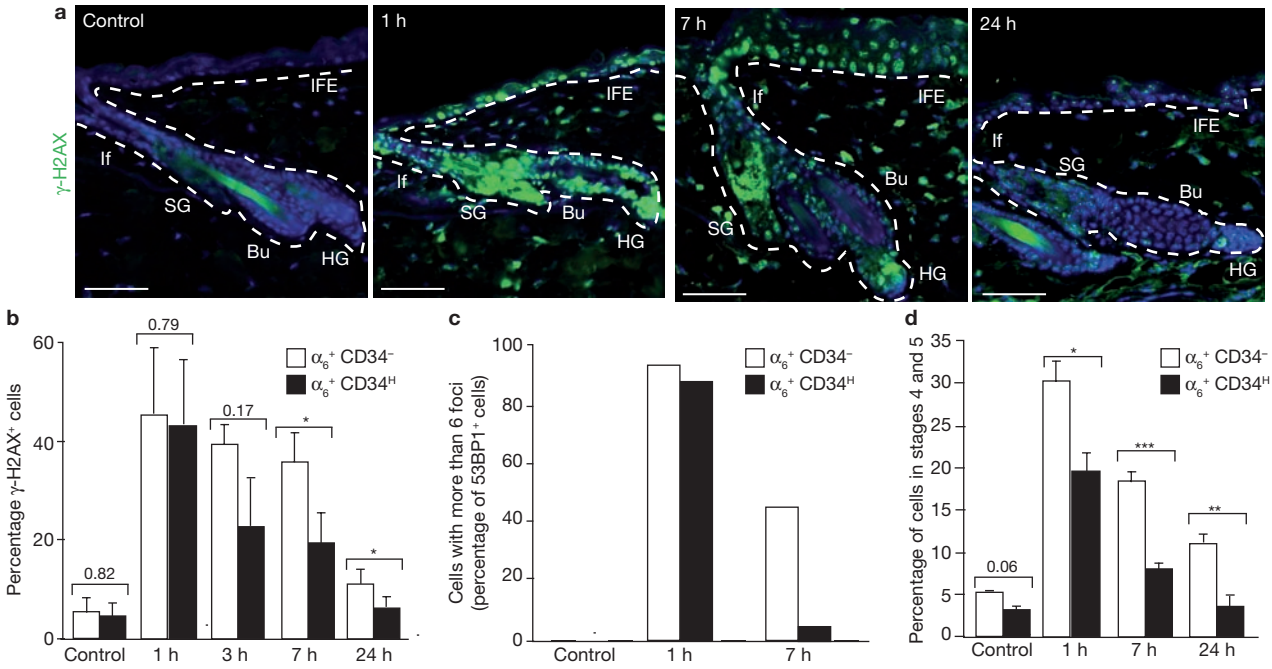

Figure 7 Bulge SCs show accelerated DNA damage repair. (**a**) Detection of DSBs by γ-H2AX staining on skin sections of 7-week-old mice at the indicated time points after 5 Gy IR, showing faster repair of DSBs in bulge SCs. (**b**) Quantification of the γ-H2AX-positive cells on Cytospin slides of FACS-isolated cells from control mice and mice receiving 5 Gy IR (error bars indicate s.e.m.; $n = 600$ cells per time point per experiment). (**c**) Quantification of cells with increased levels of DNA damage (more than six foci of 53BP1) in FACS-isolated α_6^+ CD34$^-$ and α_6^+ CD34^H cells at 1 and 7 h after 5 Gy IR (error bars indicate s.e.m.; $n = 1{,}000$ cells per time point). (**d**) Histogram illustrating cells with high levels of DNA damage (stages 4 and 5) quantified by neutral comet assay of FACS-isolated cells from mice treated or not with IR (error bars indicate s.e.m.; $n = 200$ cells per time point from three experiments). Scale bars, 50 μm. IFE, interfollicular epidermis; SG, sebaceous gland; Bu, bulge; HG, hair germ; If, infundibulum; asterisk, $P < 0.05$; two asterisks, $P < 0.01$; three asterisks, $P < 0.001$.

(Supplementary Information, Fig. S7f), the number of GFP-expressing cells within tdTomato-positive cells was higher in bulge SCs (Fig. 8a). Using another assay that detects the capacity of nuclear protein extracts to ligate linearized plasmids and form multimers of DNA fragments, we found that nuclear extracts of bulge SCs converted most monomeric DNA fragments into multimers, whereas most DNA fragments remained in a monomeric form in the reactions containing nuclear extracts from non-bulge epidermal cells (Fig. 8b). The results of these two independent NHEJ assays show that bulge SCs have a higher rate of basal NHEJ activity.

DNA-PK is one of the key proteins of the NHEJ repair pathway[32]. Despite comparable basal expressions of DNA-PK transcript and total protein (Supplementary Information, Fig. S7g, h), we found that bulge SCs showed higher nuclear expression of DNA-PK (Fig. 8c), resulting in a threefold higher nuclear DNA-PK activity (Fig. 8d). To determine whether the higher DNA-PK activity of bulge SCs is responsible for the faster DNA repair and subsequently the enhanced resistance to DNA-damage-induced apoptosis, we administered IR to severe combined immunodeficiency (SCID) mice, which harbour a point mutation in the gene encoding DNA-PK[33]. This mutation results in a roughly 50% decrease in DNA-PK activity[34] and increased DNA-damage-induced apoptosis[35,36]. In contrast with control mice, bulge SCs of SCID mice had a defect in their DNA repair activity, as revealed by the presence of numerous foci of γ-H2AX at 24 h after IR (Fig. 8e). The presence of unrepaired DNA lesions was accompanied by a sustained expression of p53 (Fig. 8f and Supplementary Information, Fig. S7i) correlated with an increased apoptosis of bulge SCs (Fig. 8g, h). The exacerbated apoptotic response of bulge SCs of SCID mice despite the residual DNA-PK activity indicates that DNA-PK activity could be rate-limiting in NHEJ activity and DNA-damage-induced apoptosis in bulge SCs. Consistent with this notion is the fact that mice heterozygous for the SCID mutation in three different genetic backgrounds (CD1, Balb/C and C57Bl/6) showed an increased IR-induced apoptotic response in bulge SCs (Fig. 8h and Supplementary Information, Fig. S7j).

DISCUSSION

Adult SCs seem to have developed different strategies to respond to DNA damage. Whereas intestinal SCs undergo massive apoptosis in response to IR[37,38] and melanocyte SCs[19] undergo premature differentiation within their niche after DNA damage, HF bulge SCs are, in contrast, profoundly resistant to apoptosis and do not differentiate or undergo senescence after IR.

It is generally assumed that that sensitivity to IR-induced cell death is related to cell proliferation[17]. However, our results suggest that the resistance to DNA-damage-induced apoptosis of bulge SCs is not correlated with their relative quiescence. The most quiescent intestinal SCs[39,40] are the most radiosensitive, followed by the actively cycling SCs[38], whereas the most rapidly cycling transit amplifying intestinal cells are the most radioresistant[38,41,42], suggesting that apoptotic sensitivity of intestinal and HF SCs to IR is not correlated with their relative quiescence.

Despite the relative radioresistance of epidermis, radiotherapy very frequently induces side effects in human epidermis (transient alopecia, acute and chronic dermatitis, and skin cancers) in patients undergoing radiotherapy, demonstrating that, although more radioresistant than other tissues, the epidermis is sufficiently radiosensitive to show physiological and

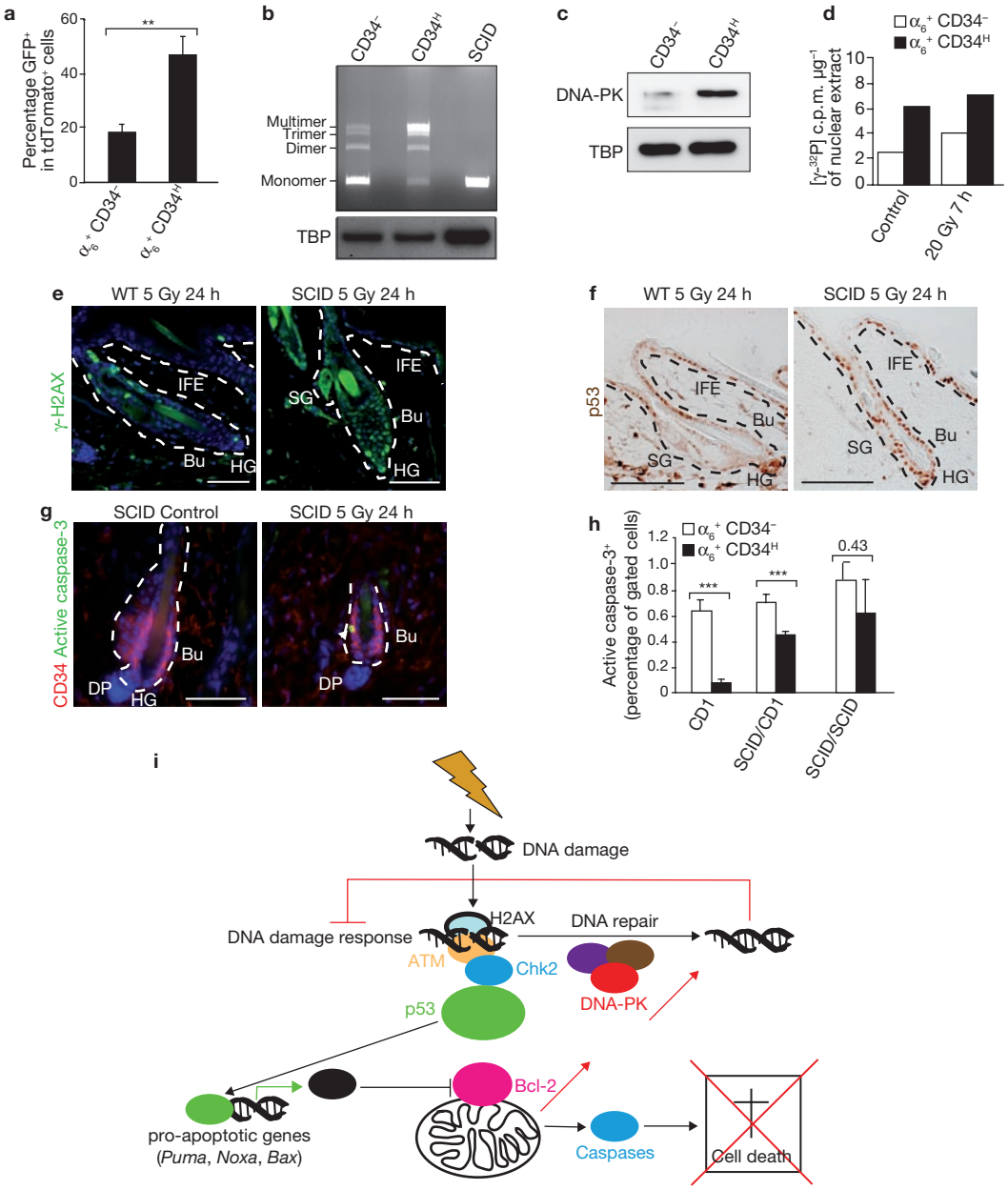

Figure 8 Higher DNA-PK activity in bulge SCs leads to more efficient NHEJ activity and protects bulge SCs from DNA-damage-induced apoptosis. (**a**) Efficiency of NHEJ as estimated by the ability to repair linearized GFP reporter plasmids. Co-transfection with tdTomato-expressing plasmids was used as an electroporation control (error bars indicate s.e.m.; $n = 8$ mice; 20,000 bulge cells per mouse). (**b**) Analysis of NHEJ efficiency in end-joining reactions containing linearized plasmid and nuclear extracts isolated from CD34$^-$ and CD34^H cells from WT mice, or total epidermal cells from SCID mice. TATA-binding protein (TBP) was used as a loading control for nuclear protein. (**c**) DNA-PK expression assessed by western blot analysis in nuclear extracts of CD34$^-$ and CD34^H cells. TBP was used as a loading control. Note the much higher nuclear expression of DNA-PK in bulge SCs. Uncropped images of blots are shown in Supplementary Information, Fig. S8c. (**d**) DNA-PK activity measured by phosphorylation of a peptide substrate by nuclear extracts of FACS-isolated cells from control and irradiated mice ($n = 2$). (**e**) γ-H2AX immunofluorescence of WT and SCID mice, showing the persistence of DSBs in bulge SCs of SCID mice. (**f**) p53 expression on skin sections from SCID mice before and after IR, showing the sustained expression of p53 in bulge cells of SCID mice. (**g**) Apoptosis in WT and SCID mice 24 h after 5 Gy IR. Arrowhead indicates an apoptotic bulge SC. (**h**) Quantification of apoptosis after 5 Gy IR in WT (CD1), SCID and heterozygous SCID (SCID/CD1) mice, showing a greater increase in apoptosis within bulge SCs (error bars indicate s.e.m.; $n = 8$ mice; 20,000 bulge cells per mouse). (**i**) Schematic summary of the DDR within the skin epidermis. Bulge SCs show higher levels of Bcl-2 and DNA-PK (red arrows), resulting in accelerated DNA repair, faster downregulation of p53 stabilization and inhibition of apoptosis. Scale bars, 50 μm. IFE, interfollicular epidermis; SG, sebaceous gland; Bu, bulge; HG, hair germ; If, infundibulum; asterisk, $P < 0.05$; two asterisks, $P < 0.01$; three asterisks, $P < 0.001$.

clinical relevance[43,44]. The significance of the small difference in apoptotic cells between bulge SCs and the other epidermal cells is likely to be physiologically relevant, because the difference in the total number of apoptotic cells between bulge SCs and the rest of the epidermis over time is higher than the frequency of active caspase-3 positivity observed at a given time point, and the alopecia after irradiation is only transient, whereas other

side effects such as chronic ulcers can be long lasting[45]. Moreover, a similar increase in apoptosis after treatment with ultraviolet B or chemical carcinogenesis after Bcl-X_L deletion in the epidermis is associated with a significant decrease in skin cancer development[46].

The extreme sensitivity of intestinal SCs to DNA-damage-induced apoptosis has been attributed to a more robust activation of the p53 pathway[47], to lower expression levels of anti-apoptotic Bcl-2 (ref. 48) and to a lack of DNA repair activity of intestinal SCs[49]. In sharp contrast, our results show that bulge SCs are more radioresistant as a result of higher levels of Bcl-2 and enhanced DNA repair activity, leading to an attenuated p53 response (Fig. 8i). The 'altruistic suicide' of intestinal SCs can decrease the likelihood of accumulating unrepaired DNA lesions but can induce SC depletion and tissue failure after DNA damage. In contrast, the resistance of bulge SCs to apoptosis after DNA damage ensures the functionality of the tissue at the expense of genome maintenance if the DNA lesions are not repaired properly.

Our study revealed that bulge SCs repair DNA damage much faster than other epidermal cells. NHEJ is the main DNA repair pathway involved in the repair of DSBs during the G0/G1 stage of the cell cycle[2,32], and DNA-PK is one of the key proteins of the NHEJ repair pathway[32]. The higher NHEJ activity associated with higher nuclear expression and activity of DNA-PK suggests that bulge SCs are naturally primed for NHEJ repair activity. Irradiation of SCID mice induced a defect in DNA repair in bulge SCs, a sustained expression of p53 and an increase in bulge SC apoptosis after IR, which is consistent with the notion that the length and the strength of p53 stabilization is the major determinant of bulge SC apoptosis after DNA damage and that the rapidity of DNA repair contributes to the resistance of bulge SCs to apoptosis. Consistent with our observations, SCID mice show a substantial decrease in 7,12-dimethylbenz[α]anthracene/TPA-induced skin tumours, which has been attributed to an increase in apoptosis after carcinogen administration that eliminated mutated epidermal cells[50].

Hematopoietic SCs (HSCs) preferentially express some genes involved in DNA repair[51,52]. Mice deficient for *Lig4*, a critical gene of NHEJ, show major defects in hematopoiesis and long-term capacities for HSC self-renewal[53,54]. Although previous experiments with limiting dilution have previously indicated that HCSs are also more resistant to DNA-damage-induced cell death[55–57], the underlying mechanism of HSC radioresistance remains unclear and could potentially involve similar mechanisms to those of bulge SCs.

Our results indicate that the resistance to DNA damage may represent a novel characteristic of adult SCs. Further studies will be required to determine whether this characteristic of bulge SCs is a more general mechanism shared by different tissue-specific SCs. These results also show that bulge SCs are poised to repair DNA through the more error-prone NHEJ repair mechanism, possibly allowing the long-term accumulation of mutations in SCs, and suggesting that the presence of the efficient NHEJ DNA repair mechanism could be a double-edged sword for adult SCs, promoting short-term survival after DNA damage at the expense of long-term maintenance of genomic integrity. These results may have important implications for understanding the increased susceptibility of certain tissues to DNA-damage-induced tumorigenesis and ageing. □

METHODS

Methods and any associated references are available in the online version of the paper at http://www.nature.com/naturecellbiology/

Note: Supplementary Information is available on the Nature Cell Biology website.

ACKNOWLEDGEMENTS

We thank the members of the Blanpain and Vanderhaeghen laboratories for comments during the realization of this study. We thank V. de Maertelaer for help with the statistical analyses. C.B. is a *chercheur qualifié* of the Fonds de la Recherche Scientifique (F.R.S.)/Fonds National de la Recherche Scientifique (FNRS). A.C. is a research fellow of the F.R.S./Fonds pour la formation à la Recherche dans l'Industrie et dans l'Agriculture (FRIA). This work was supported by a 'mandat d'impulsion scientifique' of the FNRS, a career development award of the Human Frontier Science Program Organization (HFSPO), a research grant of the Schlumberger Foundation, the programme CIBLES of the Wallonia Region, a research grant from the Fondation Contre le Cancer and the fond Gaston Ithier, a starting grant of the European Research Council (ERC) and the EMBO Young Investigator Program.

AUTHOR CONTRIBUTIONS

C.B., P.A.S., A.C., S.D.C., G.D. and J.C.M. designed the experiments and performed data analysis. P.A.S., A.C., K.K.Y., G.M. and G.L. performed most of the experiments. S.D.C., G.D. and JC.M. performed the western blot analysis. E.D. and C.S. provided technical support. C.B. and P.A.S. wrote the manuscript.

COMPETING FINANCIAL INTERESTS

The authors declare no competing financial interests.

Published online at http://www.nature.com/naturecellbiology
Reprints and permissions information is available online at http://npg.nature.com/reprintsandpermissions/

1. Rossi, D. J., Jamieson, C. H. & Weissman, I. L. Stems cells and the pathways to aging and cancer. *Cell* **132,** 681–696 (2008).
2. Garinis, G. A., van der Horst, G. T., Vijg, J. & Hoeijmakers, J. H. DNA damage and ageing: new-age ideas for an age-old problem. *Nat. Cell Biol.* **10,** 1241–1247 (2008).
3. Harper, J. W. & Elledge, S. J. The DNA damage response: ten years after. *Mol. Cell* **28,** 739–745 (2007).
4. Hoeijmakers, J. H. Genome maintenance mechanisms for preventing cancer. *Nature* **411,** 366–374 (2001).
5. Harrison, J. C. & Haber, J. E. Surviving the breakup: the DNA damage checkpoint. *Annu. Rev. Genet.* **40,** 209–235 (2006).
6. O'Driscoll, M. & Jeggo, P. A. The role of double-strand break repair — insights from human genetics. *Nature Rev. Genet.* **7,** 45–54 (2006).
7. Wyman, C. & Kanaar, R. DNA double-strand break repair: all's well that ends well. *Annu. Rev. Genet.* **40,** 363–383 (2006).
8. d'Adda di Fagagna, F. Living on a break: cellular senescence as a DNA-damage response. *Nature Rev. Cancer* **8,** 512–522 (2008).
9. Riley, T., Sontag, E., Chen, P. & Levine, A. Transcriptional control of human p53-regulated genes. *Nature Rev. Mol. Cell Biol.* **9,** 402–412 (2008).
10. Morrison, S. J. & Spradling, A. C. Stem cells and niches: mechanisms that promote stem cell maintenance throughout life. *Cell* **132,** 598–611 (2008).
11. Blanpain, C. & Fuchs, E. Epidermal homeostasis: a balancing act of stem cells in the skin. *Nature Rev. Mol. Cell Biol.* **10,** 207–217 (2009).
12. Trempus, C. S. *et al.* Enrichment for living murine keratinocytes from the hair follicle bulge with the cell surface marker CD34. *J. Invest. Dermatol.* **120,** 501–511 (2003).
13. Blanpain, C., Lowry, W. E., Geoghegan, A., Polak, L. & Fuchs, E. Self-renewal, multipotency, and the existence of two cell populations within an epithelial stem cell niche. *Cell* **118,** 635–648 (2004).
14. Tumbar, T. *et al.* Defining the epithelial stem cell niche in skin. *Science* **303,** 359–363 (2004).
15. Morris, R. J. *et al.* Capturing and profiling adult hair follicle stem cells. *Nat. Biotechnol.* **22,** 411–417 (2004).
16. Weil, M. M., Amos, C. I., Mason, K. A. & Stephens, L. C. Genetic basis of strain variation in levels of radiation-induced apoptosis of thymocytes. *Radiat. Res.* **146,** 646–651 (1996).
17. Gudkov, A. V. & Komarova, E. A. The role of p53 in determining sensitivity to radiotherapy. *Nature Rev. Cancer* **3,** 117–129 (2003).
18. Wilson, C. *et al.* Cells within the bulge region of mouse hair follicle transiently proliferate during early anagen: heterogeneity and functional differences of various hair cycles. *Differentiation* **55,** 127–136 (1994).
19. Inomata, K. *et al.* Genotoxic stress abrogates renewal of melanocyte stem cells by triggering their differentiation. *Cell* **137,** 1088–1099 (2009).
20. Youssef, K. K. *et al.* Identification of the cell lineage at the origin of basal cell carcinoma. *Nat. Cell Biol.* **12,** 299–305 (2010).
21. Song, S. & Lambert, P. F. Different responses of epidermal and hair follicular cells to radiation correlate with distinct patterns of p53 and p21 induction. *Am. J. Pathol.* **155,** 1121–1127 (1999).
22. Botchkarev, V. A. *et al.* p53 is essential for chemotherapy-induced hair loss. *Cancer Res.* **60,** 5002–5006 (2000).
23. Michalak, E., Villunger, A., Erlacher, M. & Strasser, A. Death squads enlisted by the tumour suppressor p53. *Biochem. Biophys. Res. Commun.* **331,** 786–798 (2005).
24. Youle, R. J. & Strasser, A. The BCL-2 protein family: opposing activities that mediate cell death. *Nature Rev. Mol. Cell Biol.* **9,** 47–59 (2008).

25. Stenn, K. S., Lawrence, L., Veis, D., Korsmeyer, S. & Seiberg, M. Expression of the bcl-2 protooncogene in the cycling adult mouse hair follicle. *J. Invest. Dermatol.* **103,** 107–111 (1994).
26. Michaelidis, T. M. *et al.* Inactivation of bcl-2 results in progressive degeneration of motoneurons, sympathetic and sensory neurons during early postnatal development. *Neuron* **17,** 75–89 (1996).
27. Mendrysa, S. M. *et al.* mdm2 is critical for inhibition of p53 during lymphopoiesis and the response to ionizing irradiation. *Mol. Cell. Biol.* **23,** 462–472 (2003).
28. Harris, S. L. & Levine, A. J. The p53 pathway: positive and negative feedback loops. *Oncogene* **24,** 2899–2908 (2005).
29. Siliciano, J. D. *et al.* DNA damage induces phosphorylation of the amino terminus of p53. *Genes Dev.* **11,** 3471–3481 (1997).
30. Bonner, W. M. *et al.* γH2AX and cancer. *Nature Rev. Cancer* **8,** 957–967 (2008).
31. Schultz, L. B., Chehab, N. H., Malikzay, A. & Halazonetis, T. D. p53 binding protein 1 (53BP1) is an early participant in the cellular response to DNA double-strand breaks. *J. Cell Biol.* **151,** 1381–1390 (2000).
32. Hakem, R. DNA-damage repair; the good, the bad, and the ugly. *EMBO J.* **27,** 589–605 (2008).
33. Araki, R. *et al.* Nonsense mutation at Tyr-4046 in the DNA-dependent protein kinase catalytic subunit of severe combined immune deficiency mice. *Proc. Natl Acad. Sci. USA* **94,** 2438–2443 (1997).
34. Woo, R. A., McLure, K. G., Lees-Miller, S. P., Rancourt, D. E. & Lee, P. W. DNA-dependent protein kinase acts upstream of p53 in response to DNA damage. *Nature* **394,** 700–704 (1998).
35. Biedermann, K. A., Sun, J. R., Giaccia, A. J., Tosto, L. M. & Brown, J. M. *scid* mutation in mice confers hypersensitivity to ionizing radiation and a deficiency in DNA double-strand break repair. *Proc. Natl Acad. Sci. USA* **88,** 1394–1397 (1991).
36. Fulop, G. M. & Phillips, R. A. The *scid* mutation in mice causes a general defect in DNA repair. *Nature* **347,** 479–482 (1990).
37. Potten, C. S., Wilson, J. W. & Booth, C. Regulation and significance of apoptosis in the stem cells of the gastrointestinal epithelium. *Stem Cells* **15,** 82–93 (1997).
38. Barker, N. *et al.* Identification of stem cells in small intestine and colon by marker gene *Lgr5*. *Nature* **449,** 1003–1007 (2007).
39. Marshman, E., Booth, C. & Potten, C. S. The intestinal epithelial stem cell. *BioEssays* **24,** 91–98 (2002).
40. Sangiorgi, E. & Capecchi, M. R. Bmi1 is expressed *in vivo* in intestinal stem cells. *Nat. Genet.* **40,** 915–920 (2008).
41. Wilson, J. W., Pritchard, D. M., Hickman, J. A. & Potten, C. S. Radiation-induced p53 and $p21^{WAF-1/CIP1}$ expression in the murine intestinal epithelium: apoptosis and cell cycle arrest. *Am. J. Pathol.* **153,** 899–909 (1998).
42. Potten, C. S., Owen, G. & Booth, D. Intestinal stem cells protect their genome by selective segregation of template DNA strands. *J. Cell Sci.* **115,** 2381–2388 (2002).
43. Fitzgerald, T. J. *et al.* Radiation therapy toxicity to the skin. *Dermatol. Clin.* **26,** 161–172, ix (2008).
44. Stone, H. B., Coleman, C. N., Anscher, M. S. & McBride, W. H. Effects of radiation on normal tissue: consequences and mechanisms. *Lancet Oncol.* **4,** 529–536 (2003).
45. Dorr, W. Skin and other reactions to radiotherapy — clinical presentation and radiobiology of skin reactions. *Front. Radiat. Ther. Oncol.* **39,** 96–101 (2006).
46. Kim, D. J. *et al.* Targeted disruption of Bcl-x_L in mouse keratinocytes inhibits both UVB- and chemically induced skin carcinogenesis. *Mol. Carcinog.* **48,** 873–885 (2009).
47. Merritt, A. J. *et al.* The role of p53 in spontaneous and radiation-induced apoptosis in the gastrointestinal tract of normal and p53-deficient mice. *Cancer Res.* **54,** 614–617 (1994).
48. Merritt, A. J. *et al.* Differential expression of bcl-2 in intestinal epithelia. Correlation with attenuation of apoptosis in colonic crypts and the incidence of colonic neoplasia. *J. Cell Sci.* **108,** 2261–2271 (1995).
49. Potten, C. S. Radiation, the ideal cytotoxic agent for studying the cell biology of tissues such as the small intestine. *Radiat. Res.* **161,** 123–136 (2004).
50. Kemp, C. J., Vo, K. & Gurley, K. E. Resistance to skin tumorigenesis in DNAPK-deficient SCID mice is not due to immunodeficiency but results from hypersensitivity to TPA-induced apoptosis. *Carcinogenesis* **20,** 2051–2056 (1999).
51. Ramalho-Santos, M., Yoon, S., Matsuzaki, Y., Mulligan, R. C. & Melton, D. A. 'Stemness': transcriptional profiling of embryonic and adult stem cells. *Science* **298,** 597–600 (2002).
52. Ivanova, N. B. *et al.* A stem cell molecular signature. *Science* **298,** 601–604 (2002).
53. Rossi, D. J. *et al.* Deficiencies in DNA damage repair limit the function of haematopoietic stem cells with age. *Nature* **447,** 725–729 (2007).
54. Nijnik, A. *et al.* DNA repair is limiting for haematopoietic stem cells during ageing. *Nature* **447,** 686–690 (2007).
55. Ploemacher, R. E., van Os, R., van Beurden, C. A. & Down, J. D. Murine haemopoietic stem cells with long-term engraftment and marrow repopulating ability are more resistant to gamma-radiation than are spleen colony forming cells. *Int. J. Radiat. Biol.* **61,** 489–499 (1992).
56. Meijne, E. I. *et al.* The effects of x-irradiation on hematopoietic stem cell compartments in the mouse. *Exp. Hematol.* **19,** 617–623 (1991).
57. Down, J. D., Boudewijn, A., van Os, R., Thames, H. D. & Ploemacher, R. E. Variations in radiation sensitivity and repair among different hematopoietic stem cell subsets following fractionated irradiation. *Blood* **86,** 122–127 (1995).

METHODS

Mice. CD1, Balb/c, C57BL/6, FVB/N and NOD/SCID mice were obtained from Charles River. Heterozygous SCID mice were obtained by crossing SCID mice with CD1, Balb/c or C57BL6 mice. *Mdm2* hypomorphic and *mdm2*$^{+/-}$ mice were obtained from S. M. Mendrysa (Department of Oncology, University of Wisconsin, Madison, Wisconsin) and crossed to obtain *mdm2*$^{hypo/-}$ mice. *p53*$^{fl/fl}$ mice were derived from the National Cancer Institute at Frederick. K14Cre mice were a gift from E. Fuchs (Howard Hughes Medical Institute, The Rockefeller University, New York). *Bcl-2* KO mice were a gift from M. Sendtner (Institute of Clinical Neurobiology, University of Würzburg, Würzburg, Germany). K19CreER knock-in mice were provided by Guoqiang Gu (The Vanderbilt University Medical Center, Nashville, Tennessee). Rosa–YFP mice were obtained from the Jackson Laboratory. All animal experiments were performed in accordance with the guidelines of the Université Libre de Bruxelles and the Ethical Committee for Animal Welfare (reference number 260N).

Animal treatments. Mice received total-body irradiation from a ^{137}Cs source in a Mark I 68A irradiator (J. L. Shepherd & Associates). TPA (Sigma-Aldrich), diluted in acetone, was applied topically once a day at 700 pg kg^{-1}. BrdU (Sigma-Aldrich) was injected intraperitoneally at 50 mg kg^{-1} at 4 h before the mice were killed. Tamoxifen was injected intraperitoneally in 200 µl of 9:1 sunflower oil/ethanol.

Antibodies. The following antibodies were used. For immunofluorescence: anti-P-cadherin (1:200 dilution; Zymed), anti-GFP (1:1,000), anti-Tenascin C (1:1,000), anti-Ki67 (1:1,000) and anti-BrdU (1:400) all from Abcam, anti-β_4 integrin (1:200; BD Biosciences), anti-Sox9 (1:1,000; Chemicon), anti-K15 (1:10,000), anti-K10 (1:1,000), anti-K1 (1:1,000), anti-Loricrin (1:1,000) and anti-K14 (1:2,000) all from Covance, anti-Lrig1 (1:1,000; R&D Systems), anti-Gata3 (1:100, Santa Cruz), anti-(active caspase-3) (1:600; R&D Systems), anti-CD34 (1:100; eBiosciences), anti-γ-H2AX (1:600; Millipore), anti-53BP1 (1:500; Novus Biological), anti-rat, anti-mouse, anti-goat, anti-chicken and anti-rabbit conjugated with Alexa-488 (1:400; Invitrogen), anti-rat and anti-rabbit conjugated with rhodamin red-X (RRX; 1:400; Jackson Immunoresearch); anti-MTS24 (1:200) was a gift from Richard Boyd (Monash Immunology and Stem Cell). For FACS analysis: biotinylated anti-CD34 (1:50; eBiosciences), phycoerythrin-conjugated anti-α_6 integrin (1:50), fluorescein isothiocyanate (FITC)-conjugated anti-BrdU (1:50) and FITC-conjugated anti-(active caspase-3) (1:50) and allophycocyanin-conjugated streptavidin (1:400), all from BD Biosciences. For western blotting: p53 (1:250; Santa Cruz), Mdm2 (1:200; Santa Cruz), pSer15-p53 (1:1,000; Cell Signaling), Bcl-2 (1:100; BD Biosciences), DNA-PK (1:200; Thermo Scientific), vinculin (1:1,000; Sigma) and TATA-binding protein (1:2,000; Abcam).

Immunofluorescence. Antigen unmasking of paraffin sections was performed in PT module (LabVision) for 20 min at 98 °C, using citrate buffer pH 6.0 for BrdU and PT Module buffer 1 for γ-H2AX (both from LabVision).

Non-specific antibody binding was blocked with 5% horse serum, 1% BSA and 0.2% Triton X-100 for 1 h at 22 °C. When mouse primary antibodies were used, non-specific antigen blocking was performed with M.O.M Basic Kit reagent (Vector). Primary antibodies were incubated overnight at 4 °C, followed by incubation of the secondary antibodies for 1 h at room temperature. Slides were mounted with Glycergel (Dako) supplemented with 2.5% 1, 4 Diazobicyclo(2, 2, 2)octane (DABCO; Sigma-Aldrich).

In Situ Cell Death Detection Fluorescein kit (Roche) was used to detect apoptosis. Cellular senescence was assessed with Senescence β-Galactosidase Staining Kit (Cell Signaling).

Immunohistochemistry. Paraffin sections were deparaffinized and rehydrated. Antigen unmasking was performed for 20 min at 98 °C in citrate buffer pH 6 using PT Module. Endogenous peroxidase was blocked with 3% H_2O_2 in methanol for 10 min at room temperature. Endogenous avidin and biotin were blocked with Endogenous Blocking Kit (Invitrogen) for 20 min at room temperature. Non-specific antigen blocking was performed with M.O.M Basic Kit reagent. Mouse anti-p53 antibody (clone 1C12; Cell Signaling) was incubated overnight at 4 °C. Anti-mouse biotinylated in M.O.M blocking kit, Standard ABC Kit and ImmPACT DAB (Vector Laboratories) were used for the detection of horseradish peroxidase activity. Slides were then dehydrated and mounted with SafeMount (Labonord).

Haematoxylin/eosin staining. Paraffin sections were deparaffinized, rehydrated, incubated with Mayer's haematoxylin for 4 min, fixed in 70% ethanol and 0.1% HCl and incubated in eosin for 20 s.

Oil Red O staining. Oil Red O staining was performed by incubation for 30 s with Oil Red O on cryosections after being fixed for 10 min with 4% PAF and permeabilized for 5 min with 60% propan-2-ol. Slides were counterstained with Mayer's haematoxylin for 2 min.

Bioimaging. All imaging was performed on a Zeiss Axio Imager.M1 (Thornwood) microscope with a Zeiss Axiocam MRm camera for immunofluorescence and Zeiss Axioxam MRC5 camera for bright-field imaging, using Axiovision release 4.6 software. Single cell pictures were acquired with a Zeiss Axio Imager.M1 supplied with a 100× objective (α-Plan-Fluor 1.45 numerical aperture oil-immersion objective). Photoshop CS3 (Adobe) was used to adjust brightness, contrast and picture size.

Quantification of p53-positive cells by immunohistochemistry. The numbers of total cells and p53-positive cells were counted for each compartment, on the basis of their histological appearance; that is, for the interfollicular epidermis (IFE), infudibulum (If), sebaceous gland (SG), bulge (Bu) and hair germ (HG) areas as indicated in all figures. The non-bulge area was defined by the sum of the cells counted in the IFE, the If and SG and the HG.

Flow cytometry and cell sorting. Isolation of keratinocytes and analysis of cell proliferation with the BrdU Flow Kit (BD Biosciences) were performed as described previously[13]. Dead cells were excluded by using Hoechst 33342 at 4 µM. FACS analysis was performed with FACSCalibur and CellQuestPro software (BD Biosciences). FACSAria sorter and FACS DiVa software (BD Biosciences) were used for cell sorting.

Magnetic-activated cell sorting. Total epidermal cells were stained with biotinylated antibody against CD34 (eBiosciences), followed by anti-biotin magnetic beads (Miltenyi), in accordance with the manufacturer's protocol. The purity of the isolated cells was assessed by FACS analysis.

Quantification of γ-H2AX on Cytospin slides. FACS-sorted α_6^+ CD34$^-$ and α_6^+ CD34^H cells, not later than 15 min after sorting, were centrifuged at 500*g* for 5 min with a Cytospin 3 centrifuge (Shandon) at 25,000 cells per slide. Cells were fixed in 4% PAF and permeabilized with prechilled 90% methanol for 53BP1 and 0.1% Triton X-100 in blocking buffer for γ-H2AX.

Reverse transcriptase and quantitative PCR. RNA extraction was performed with Absolutely RNA Microprep kit (Stratagene). Purified RNA (0.5 µg) was used to synthesize the first-strand cDNA in a final volume of 50 µl, using SuperscriptII (Invitrogen) and random hexamers (Roche). Quantitative PCR (qPCR) analyses were performed with 1/100 of the cDNA reaction as template, using a Quantifast SYBR Green mix (Qiagen) on an ABI Fast7500 Real-Time PCR system. *Hypoxanthine phosphoribosyltransferase* (*HPRT*) and *β-actin* were used as housekeeping internal reference genes. The following primers were used: *53BP1*, 5′-AGACACTCCTTGCCTGAT-3′ (forward) and 5′-GTTCCGGATTTGATACA-3′ (reverse); *Atm*, 5′-AGTCCGACCTCCATTCC-3′ (forward) and 5′-CACACCCAAGCTTTCCATCCT-3′ (reverse); *β-actin*, 5′-ACCAACTGGGACGATATGGAGAAGA-3′ (forward) and 5′-TACGACCAGAGGCATACAGGGACAA-3′ (reverse); *Bad*, 5′-GGGGACCGAGGAGGATGAAGG-3′ (forward) and 5′-GCGACGGGAGCGGGTAGAGT-3′ (reverse); *Bak*, 5′-AGCCGGGAATGCCTACGAAC-3′ (forward) and 5′-GGCCCAACAGAACCACACCA-3′ (reverse); *Bax*, 5′-CCGCGTGGTTGCCCTCTTCTAC-3′ (forward) and 5′-TTTCCCCTTCCCCCATTCATCC-3′ (reverse); *Bcl-2*, 5′-ATGGGGTGAACTGGGGGAGGATTG-3′ (forward) and 5′-GGCCAGGCTGAGCAGGGTCTTC-3′ (reverse); *Bid*, 5′-AACCGCGACCATGGAAAGACC-3′ (forward) and 5′-ATGCAGGAGCCGGCGTAAACT-3′ (reverse); *Brca1*, 5′-TGCTGCCCAAGGGTCAACTG-3′ (forward) and 5′-ACTCTCGTATCCGGATGCCTCTG-3′ (reverse); *Brca2*, 5′-CTGCTGACTCTCCCGCTACTTTG-3′ (forward) and 5′-TGTCTTGCCCATTCTCATTTTCTG-3′ (reverse); *CD34*, 5′-GGTCTTGGCCAATAGCACAG-3′ (forward) and 5′-GGAGTGCGTGTGGAGGAGGAGGAG-3′ (reverse); *Cdc25a*, 5′-CACCGCCGCCGCCTGTTCTTC-3′ (forward) and 5′-CGGTCGATTCTGAGGAGCCCATTC-3′ (reverse); *Chk2*, 5′-TTGCACGAGCTCTCAC-

DOI: 10.1038/ncb2059

AGTATCAG-3 (forward) and 5′-GTCCGTCCTTCTCAACAGTGGTC-3′ (reverse); *Col18a1*, 5′-GATGCTGCCCAGGTGGTAGTCTC-3′ (forward) and 5′-TGCCCGGTCTTCATCATCATCT-3′ (reverse); *Ctgf*, 5′-TGTGTCTTCGGTGGGTCGGTGTA-3′ (forward) and 5′-TGCGGTCCTTGGGCTCGTC-3′ (reverse); *DNA-PK*, 5′-TGCCGGGGCCAGTTACC-3′ (forward) and 5′-AGGGCTTCTTCTCTACAATCACGA-3′ (reverse); *Ercc1*, 5′-CTCCGCTACCACAACCTCCATCCA-3′ (forward) and 5′-GGTACCGCCCTGCTTCCTCTGC-3′ (reverse); *Ercc2*, 5′-GTGGCCCGGGAGACAGATG-3′ (forward) and 5′-AGAGTGGCGAAGTTAGCAAGGAGT-3′ (reverse); *Ercc3*, 5′-GTGGCGGGCCTTCTACTTC-3′ (forward) and 5′-ATCTTCCGCAGGCTCTTCTCC-3′ (reverse); *Ercc4*, 5′-AGCCGGCCGAGGAGGAATA-3′ (forward) and 5′-CGGAAGAGGCGCAGGATGA-3′ (reverse); *Ercc5*, 5′-GAGGCGCTGGAGGGCAAGGTG-3′ (forward) and 5′-CGGTGGTTTTTCTCGAGTCAATGG-3′ (reverse); *Gata3*, 5′-TCCGGCTTCATCCTCTTCTCTGG-3′ (forward) and 5′-TCGGGCACATAGGGCGGATAG-3′ (reverse); *H2AX*, 5′-CTTCACGCGCCGGCCTTCAGTTCC-3′ (forward) and 5′-CACGCCGCCCAGCAGCTTGTTGAG-3′ (reverse); *Hprt*, 5′-GCTACTGTAATGATCAGTCAACGGG-3′ (forward) and 5′-AAGCTTGCAACCTTAACCATTTTG-3′ (reverse); *Idb2*, 5′-GCAAAACCCCGGTGGACGAC-3′ (forward) and 5′-TGGTGATGCAGGCTGACGATAGTG-3′ (reverse); *Inv*, 5′-GAAGCGGCCAAACCCTGTGAA-3′ (forward) and 5′-CTGCTGCTGCTGCTGCTGTCTG-3′ (reverse); *K1*, 5′-GCCGAGCAGCGTGGTGAGAA-3′ (forward) and 5′-ACTGATGGTGGTGTGGCTGGTGTT-3′ (reverse); *K5*, 5′-CGCCGCCTCTGCCATCAC-3′ (forward) and 5′-CACCGAAGCCAAAGCCACTACC-3′ (reverse); *K10*, 5′-TGCTTTGGGGGCTCATCAGGT-3′ (forward) and 5′-GCCAGGCGGTCGTTCAGGTT-3′ (reverse); *Ku70*, 5′-TCCAGCTTGTCTTCCTCCCTTATG-3′ (forward) and 5′-AGATCTACCACTTGCTCCGACTCC-3′ (reverse); *Ku80*, 5′-GACCTCAGCAGCCCGTTCAG-3′ (forward) and 5′-CAGCCCGTCTTCGCCTTCTA-3′ (reverse); *Lig4*, 5′-CCAGGCCCGGATACATAC-3′ (forward) and 5′-ACAGGGGCCATTTCTTCAGGA-3′ (reverse); *Mcl1*, 5′-GGGGCAGGATTGTGACTCTTATTT-3′ (forward) and 5′-AGCCCCTACTCCAGCAACACC-3′ (reverse); *Mdm2*, 5′-GTCTATCGGGTCACAGTCTATCA-3′ (forward) and 5′-TTTATCTTTCCCCTTATCGTCTG-3′ (reverse); *MdmX*, 5′-AGGTCCTTGAGCGATGATACTG-3′ (forward) and 5′-AACCTGGGCTTTTCCTCCTT-3′ (reverse); *Mus81*, 5′-ATCGGCCAGCCAGGTATG-3′ (forward) and 5′-GGTTTCGCCAATGTCCAC-3′ (reverse); *nFatc1*, 5′-GGCGGGAAGAAGATGGTGCTGTC-3′ (forward) and 5′-TGGTTGCGGAAAGGTGGTATCTCA-3′ (reverse); *Noxa*, 5′-CGCTTGCTTTTGGTTCCCTGAG-3′ (forward) and 5′-CAAACGACTGCCCCCATACAAT-3′ (reverse); *p21*, 5′-CTGAGCGGCCTGAAGATT-3′ (forward) and 5′-GCTAAGGCCGAAGATGGGGAAGA-3′ (reverse); *p53*, 5′-TGCCCCAGCCACTCCAT-3′ (forward) and 5′-GGCGCTGACCCACAACTG-3′ (reverse); *P-Cadh*, 5′-GAGTCGGGCTGGCTGTTGTTG-3′ (forward) and 5′-GCTCCTTCGGCTCTTGGCTATG-3′ (reverse); *Plet1*, 5′-CGCTCCGCTCCTTGCTTCC-3′ (forward) and 5′-ACTGGGCTGTCGTCCTCCTTCA-3′ (reverse); *Ptprv*, 5′-CACCCAGGGGCCTCTCAAAAAG-3′ (forward) and 5′-TTCCCTCCTGGTCCACTCATCCTC-3′ (reverse); *Puma*, 5′-CGCCCCCACCGCTCCACCTG-3′ (forward) and 5′-CCGGGCCCACTCCTCCTCCTCCAC-3′ (reverse); *Rad51*, 5′-GTTCGCTGCAGATCCCAAAAA-3′ (forward) and 5′-GAAGCCCAGTACACAGTCCTCTCC-3′ (reverse); *S100a4*, 5′-CAGGCAAAGAGGGTGACAA-3′ (forward) and 5′-TTCTTCCGGGGCTCCTTAT-3′ (reverse); *Sox9*, 5′-GGCGGAGGAAGTCGGTGAAGA-3′ (forward) and 5′-ACGTCGGTTTTGGGAGTGGTG-3′ (reverse); *Tcf3*, 5′-GTCGCCATCTCCAGCACACTTG-3′ (forward) and 5′-TCATGGCGAGGGCAGGGTAA-3′ (reverse); *Tcf4*, 5′-CAGCTCAAAGCATCAGGACTC-3′ (forward) and 5′-TGTTGATCAAGGCCAAAGCGC-3′ (reverse); *Tnc*, 5′-ATGGGGAGTCTGCCTATGCTGTG-3′ (forward) and 5′-TTGGTGATGGCTGAGTCTGTGTCC-3′ (reverse). Analysis of results was performed with qBase and MS Excel software.

Western blot analysis. FACS-sorted cells were lysed in 50 mM HEPES pH 7.5, 150 mM NaCl, 1 mM EDTA, 2.5 mM EGTA, 2 mM dithiothreitol (DTT), 0.1% Tween 20, 1 mM phenylmethylsulphonyl fluoride, 0.4 U ml^{-1} aprotinin, 10 mM β-glycerophosphate, 1 mM NaF, 0.1 mM $NaVO_4$. Total proteins (25 μg) were loaded on acrylamide and bisacrylamide gel at 10% for p53, phospho-p53, Mdm2 and Bcl-2, at 6% for DNA-PK, and 4–12% gradient for γ-H2AX. Proteins were then transferred to poly(vinylidene difluoride) membranes. Enhanced chemiluminescence (ECL) anti-mouse and anti-rabbit IgG conjugated with horseradish peroxidase (1:10,000; Healthcare) were used as secondary antibodies.

Single-cell gel electrophoresis (neutral comet assay). FACS-sorted α_6^+ $CD34^-$ and α_6^+ $CD34^H$ cells were used not later than 15 min after cell sorting in neutral comet assays with the use of the OxiSelect Comet Assay Kit (Bioconnect BV). The classification of the stages of DNA damage is illustrated in Supplementary Fig. S7d.

DNA-PK kinase activity. DNA-PK kinase activity was assessed with the SignaTECT DNA-PK assay system (Promega) in 10 μg of nuclear extracts prepared using the Nuclear Extraction Kit (Active Motif) from MACS-isolated cells. Reactions were performed with or without biotinylated DNA-PK substrate and no activator was used.

NHEJ activity. Total epidermal cells were co-electroporated with pcDNA3–enhanced green fluorescent protein (EGFP) plasmid digested with *Bam*H1, which cleaves between the promoter and the EGFP open reading frame and pCMV–tdTomato at 1 μg of DNA per 10^6 cells each. Cells were then cultured for 5 h and subsequently stained for integrin α_6 and CD34. The percentage of EGFP-expressing and tdTomato-expressing cells was estimated by flow cytometry, excluding dead cells identified with Hoechst dye.

In vitro NHEJ assay was performed with nuclear extracts prepared from MACS-isolated cells. pcDNA3–EGFP plasmid was linearized by cleavage with *Bam*H1. Protein extract (40 μg) was incubated with 400 ng of DNA substrate in reaction buffer (1 mM ATP, 0.25 mM dNTP, 25 mM Tris acetate, 100 mM potassium acetate, 10 mM magnesium acetate, 1 mM DTT at pH 7.5) for 1.5 h at 37 °C. The reaction mixture was deproteinized with 1 mg ml^{-1} proteinase K at 65 °C for 30 min and separated electrophoretically on 0.5% agarose gel for 5 h at 60 V.

Statistical analysis. Statistical significance was computed with Student's *t*-test statistics, unless mentioned otherwise. The number of individuals in each experiment and the number of independent experiments are indicated in the respective figure legends.

nature cell biology

DOI: 10.1038/ncb2059

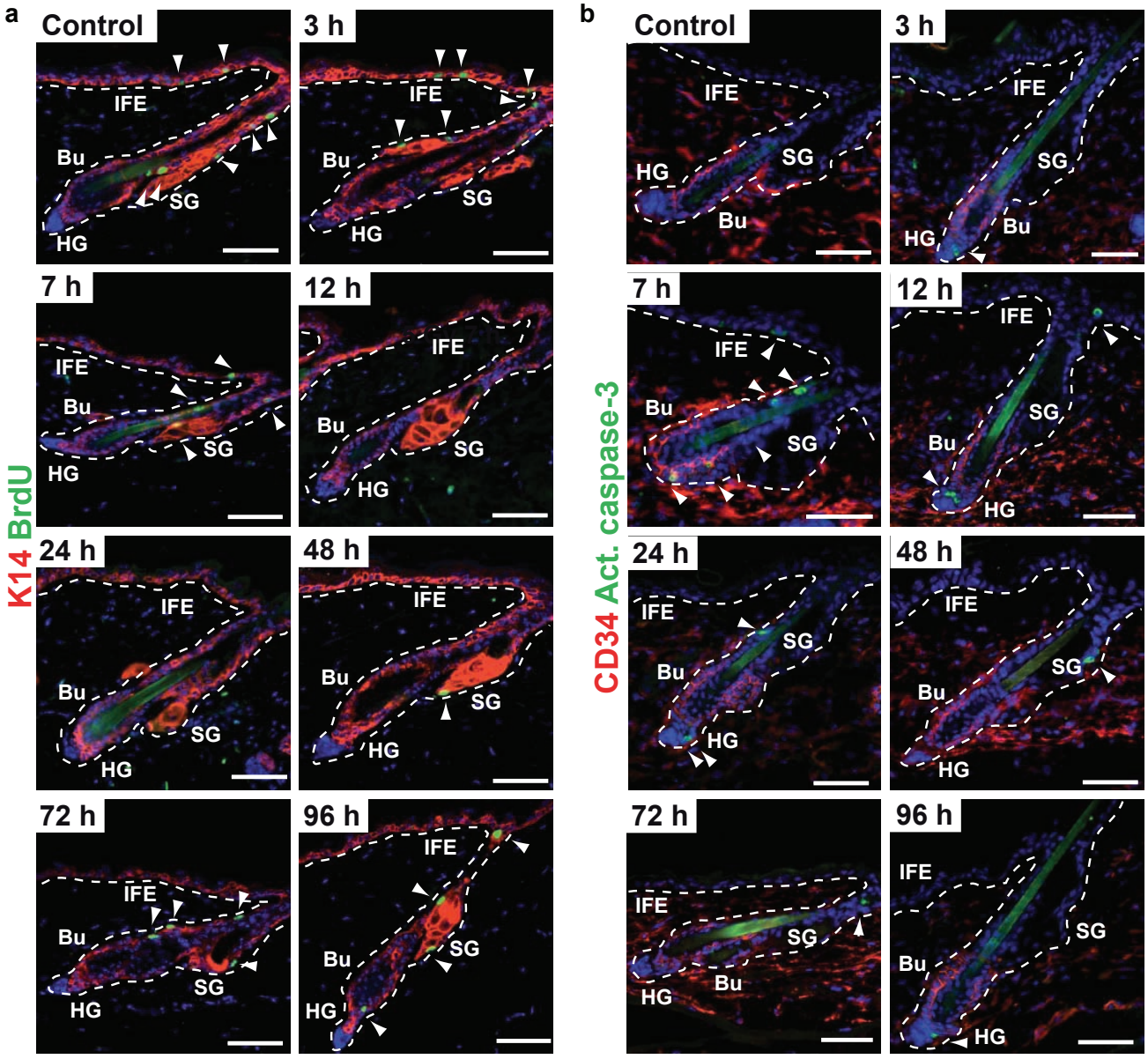

Figure S1 Kinetics of cell cycle arrest and apoptosis in mouse epidermis. **(a)** Kinetics of cell cycle arrest in 7-week old mice following 5 Gy of IR. Immunofluorescence analysis on skin sections of mice treated with BrdU for 4 h before sacrifice. The basal layer of epidermis is stained with an antibody against cytokeratin 14 (K14). **(b)** Apoptosis following 5Gy IR in 7-week old mice as determined by active caspase-3 immunofluorescence on skin sections at different time points after IR. Bulge SCs are stained with anti-CD34 antibody. Scale bars represent 50 μm (IFE, interfollicular epidermis; SG, sebaceous gland; Bu, bulge; HG, hair germ).

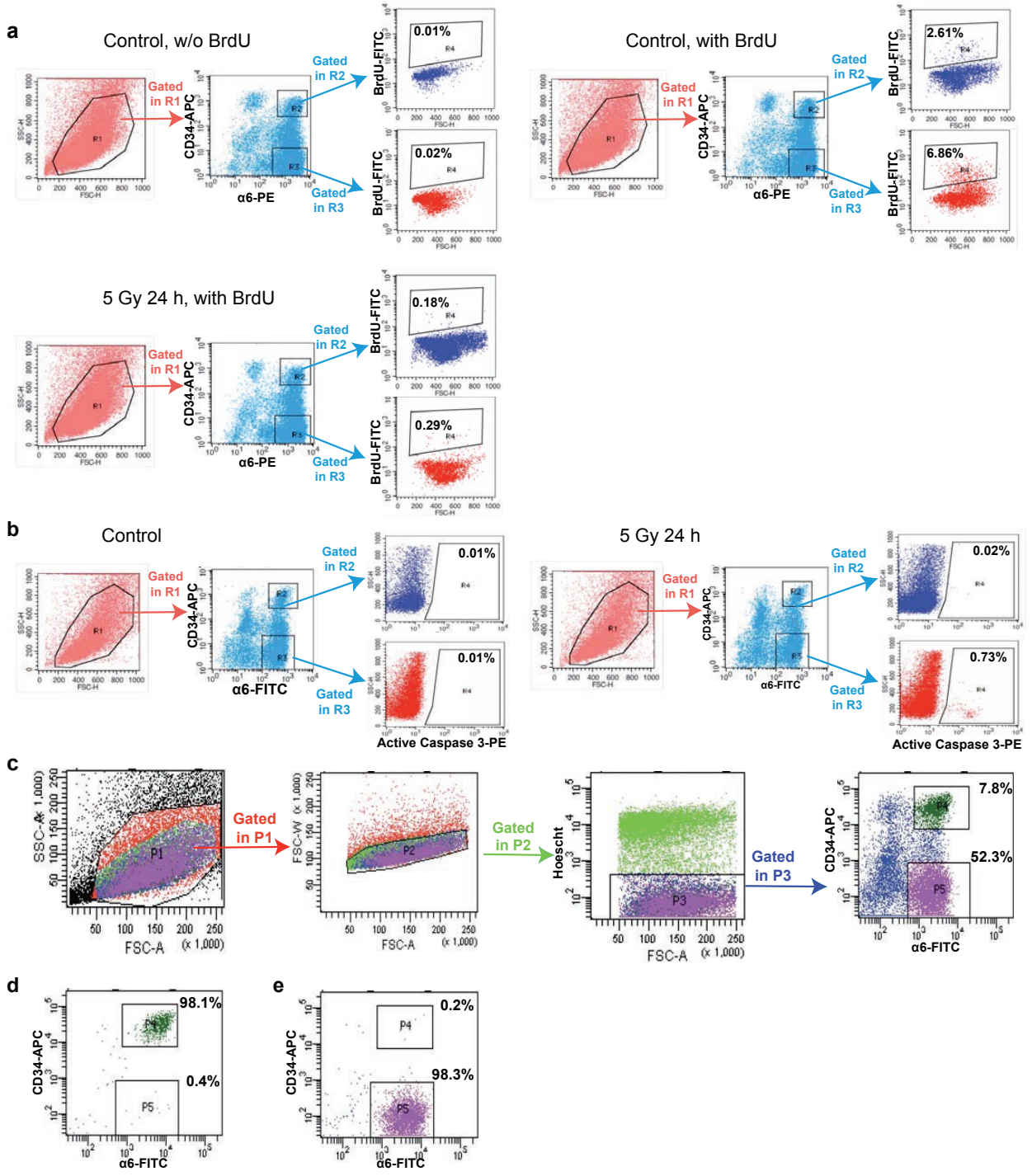

Figure S2 Gating strategy and controls for FACS analysis and cell sorting. **(a, b)** Quantification of proliferation using BrdU **(a)** and apoptosis using active caspase-3 immunostaning **(b)**. Control and irradiated mice were pulsed or not with BrdU. Their skin was dissociated into single cells and then stained with the relevant antibodies. Cells were first gated to exclude cellular debris and then bulge SCs (α6+CD34H) and the rest basal epidermal cells (α6+CD34-) were gated based on α6 and CD34 expression. Finally, α6+CD34- and α6+CD34H gated cells were analysed for BrdU incorporation (cells not pulsed with BrdU were used to set up the gate for the background of BrdU staining) **(a)** or active caspase-3 expression (control, non-irradiated cells were used to set the gate for the background of active caspase-3 staining) **(b)**. The percentage of positive cells were determined within α6+CD34- and α6+CD34H respectively. **(c-e)** Gating strategy of cell sorting and purity of the isolated populations. Suspension of epidermal cells were first gated to exclude debris, subsequently doublets were eliminated, living cells were then selected through Hoescht dye exclusion, and finally analyzed for α6 and CD34 expression. α6+CD34- and α6+CD34H- gated cells were then sorted **(c)**. Post-sort purity of α6+CD34H **(d)** and α6+CD34- **(e)** isolated cells.

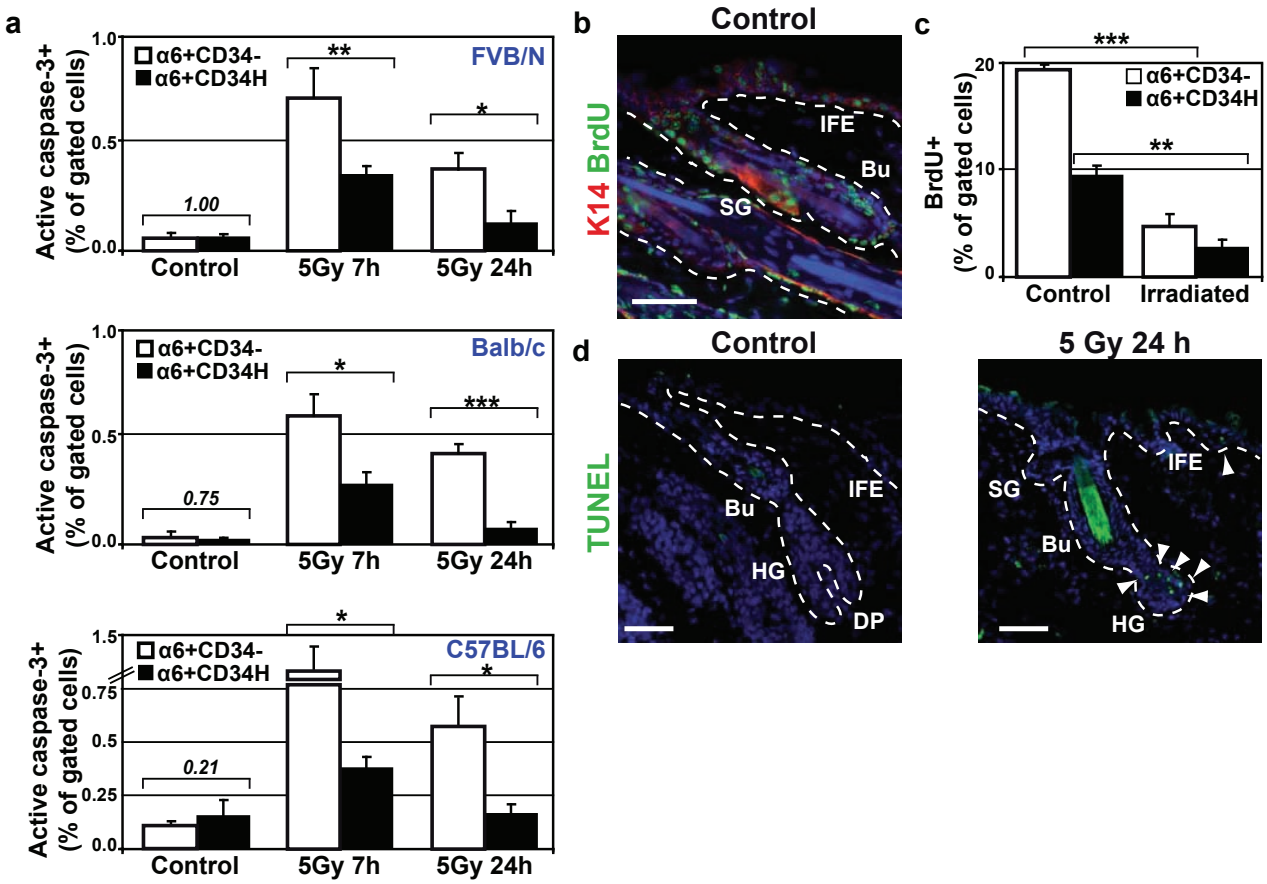

Figure S3 Resistance of bulge SCs to apoptosis is not dependent on the mouse genetic background and the proliferation state of the SCs **(a)** Quantification of apoptosis by FACS analysis before or following 5 Gy IR in FVB/N (upper panel), Balb/c (middle panel) and C57BL/6 (lower panel) mice, showing that the mouse genetic background does not influence the radioresistance of bulge SCs (error bars, s.e.m.; n=5 mice; 20000 bulge cells/mouse). **(b)** Analysis of cell proliferation during HF regeneration by IF. 23-day old mice were pulsed with BrdU twice daily for 3 days, and skin sections were stained with BrdU and K14. Note that bulge SCs incorporate BrdU during this stage of the hair cycle. **(c)** Quantification by FACS analysis of the BrdU incorporation of bulge SCs and the rest basal epidermal cells in control and irradiated mice treated with TPA as presented in **(c)** (error bars, s.e.m.; n = 5 mice; 20000 bulge cells/mouse). **(d)** Apoptosis as determined by TUNEL staining in skin sections of 23-day old mice after receiving 5 Gy IR. Apoptotic cells, stained in green, are pointed by arrowheads. Scale bars represent 50 μm (IFE, interfollicular epidermis; SG, sebaceous gland; Bu, bulge; HG, hair germ; asterisks indicate *$p < 0.05$, **$p < 0.01$, ***$p < 0.001$).

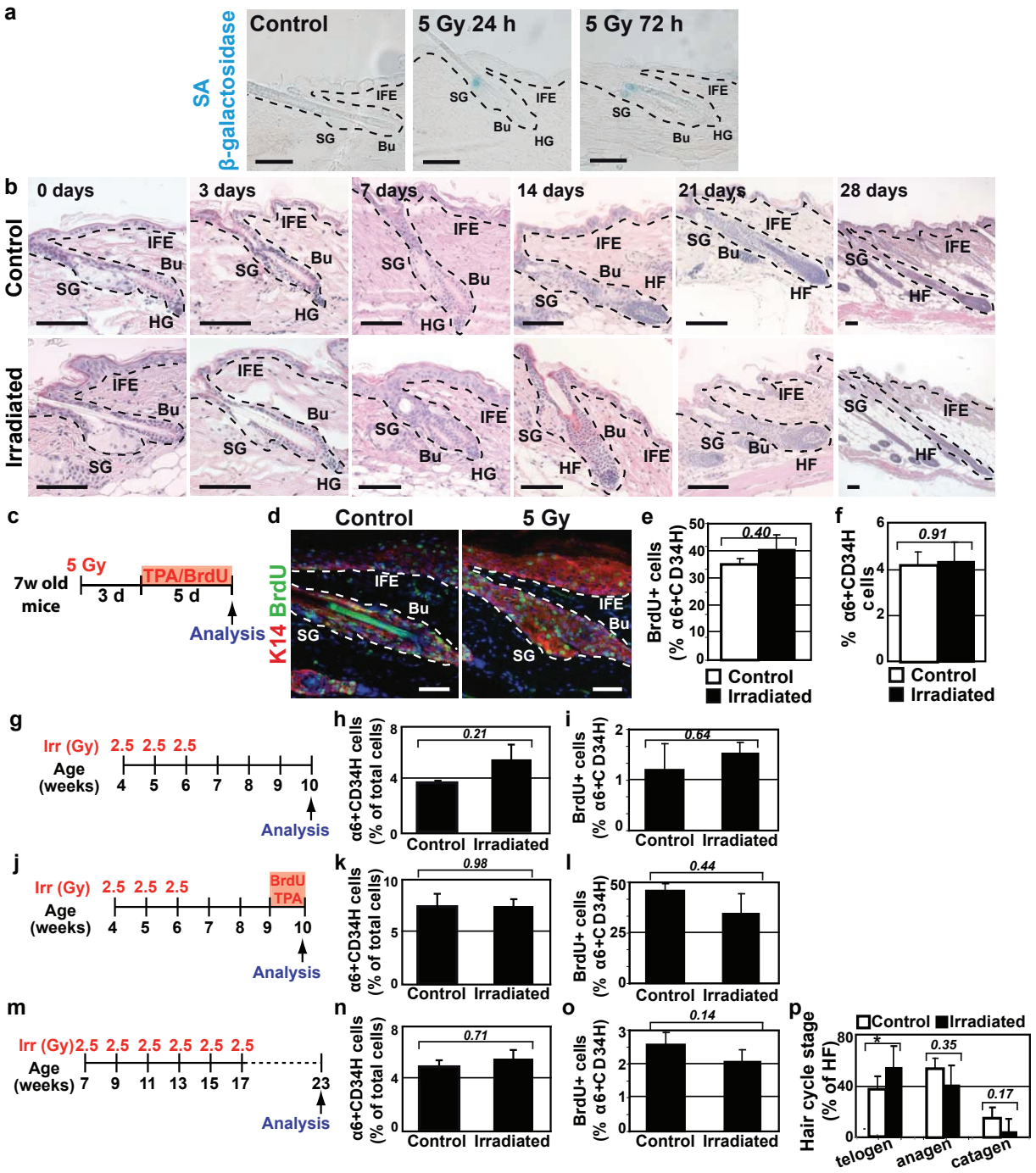

Figure S4 Bulge SCs do not undergo senescence upon DNA damage **(a)** Senescence associated β-galactosidase staining of skin sections before, 24 and 72 h after 5 Gy IR. Note the β-galactosidase positive cells in the sebaceous gland post-IR. **(b)** Hair cycle stages as determined by hematoxylin/eosin staining in control and irradiated mice. **(c)** Scheme illustrating the protocol used to study the response of bulge SCs to proliferative stimulus after DNA damage. **(d-f)** BrdU incorporation of bulge SCs (α6+CD34H) as determined by IF **(d)** and FACS analysis **(e)** and the percentage of bulge SCs within the total basal epidermal cells **(f)** in mice treated as presented in **(c)** (error bars, s.e.m.; n = 4 mice; 500000 total cells/mouse). **(g, j, m)** Schemes illustrating the protocols used to study the effect of repeated doses of IR on mouse epidermis short term after IR with **(j)** or without **(g)** TPA treatment or long term after IR **(m)**. **(h, k, n)** Quantification of the percentage of bulge SCs (α6+CD34H) in mice treated respectively as presented in **(g)**, **(j)** and **(m)** (error bars, s.e.m.; n 4-5 mice; 500000 total cells/mouse). **(i, l, o)** Quantification of the proliferation potential by FACS analysis of BrdU incorporation in mice treated respectively as presented in **(g, j, m)** (error bars, s.e.m.; n = 5 mice; 500000 total cells/mouse). **(p)** Quantification of the HFs in the different stages of hair cycle in the control and irradiated animals presented in **(m)** (error bars, s.e.m.; n =5 mice; 100 follicular units/mouse). Scale bars represent 50 μm (IFE, interfollicular epidermis; SG, sebaceous gland; Bu, bulge; HG, hair germ). Asterisks indicate *p < 0.05.

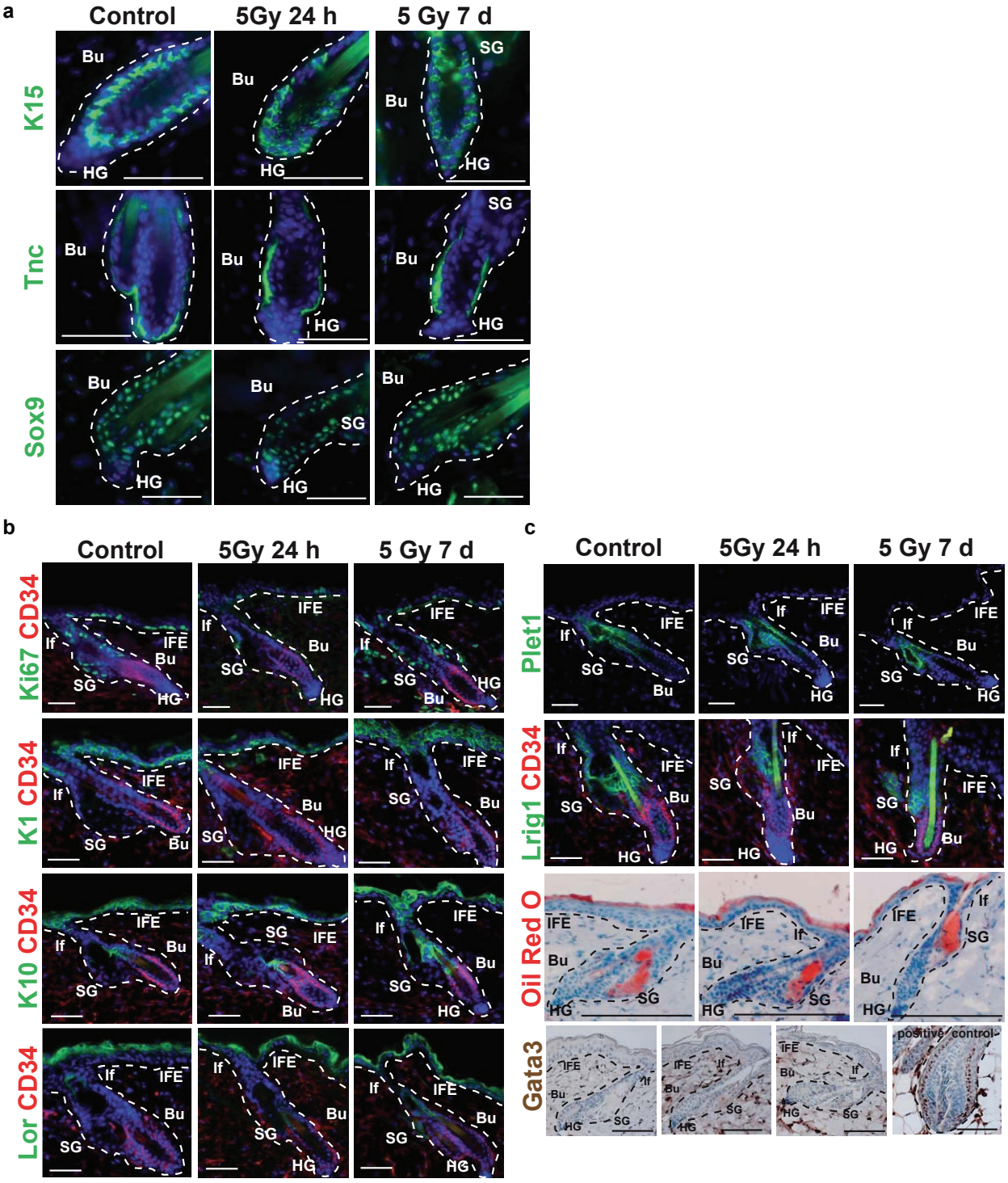

Figure S5 Bulge SCs maintain the expression of bulge SC markers and do not differentiate upon irradiation. **(a)** Analysis of bulge specific markers on skin sections of control and irradiated mice 24 h and 7 days after 5 Gy IR. **(b, c)** Analysis of the differentiation markers for the various lineages of epidermal cells on skin sections in control and irradiated mice 24 h and 7 days after 5 Gy IR. Note the absence of expression of the differentiation markers in bulge SCs before and after IR. Scale bars represent 50 μm. IFE, interfollicular epidermis; SG,sebaceous gland; Bu, bulge; HG, hair germ; If, infundibulum. Antibodies are color-coded.

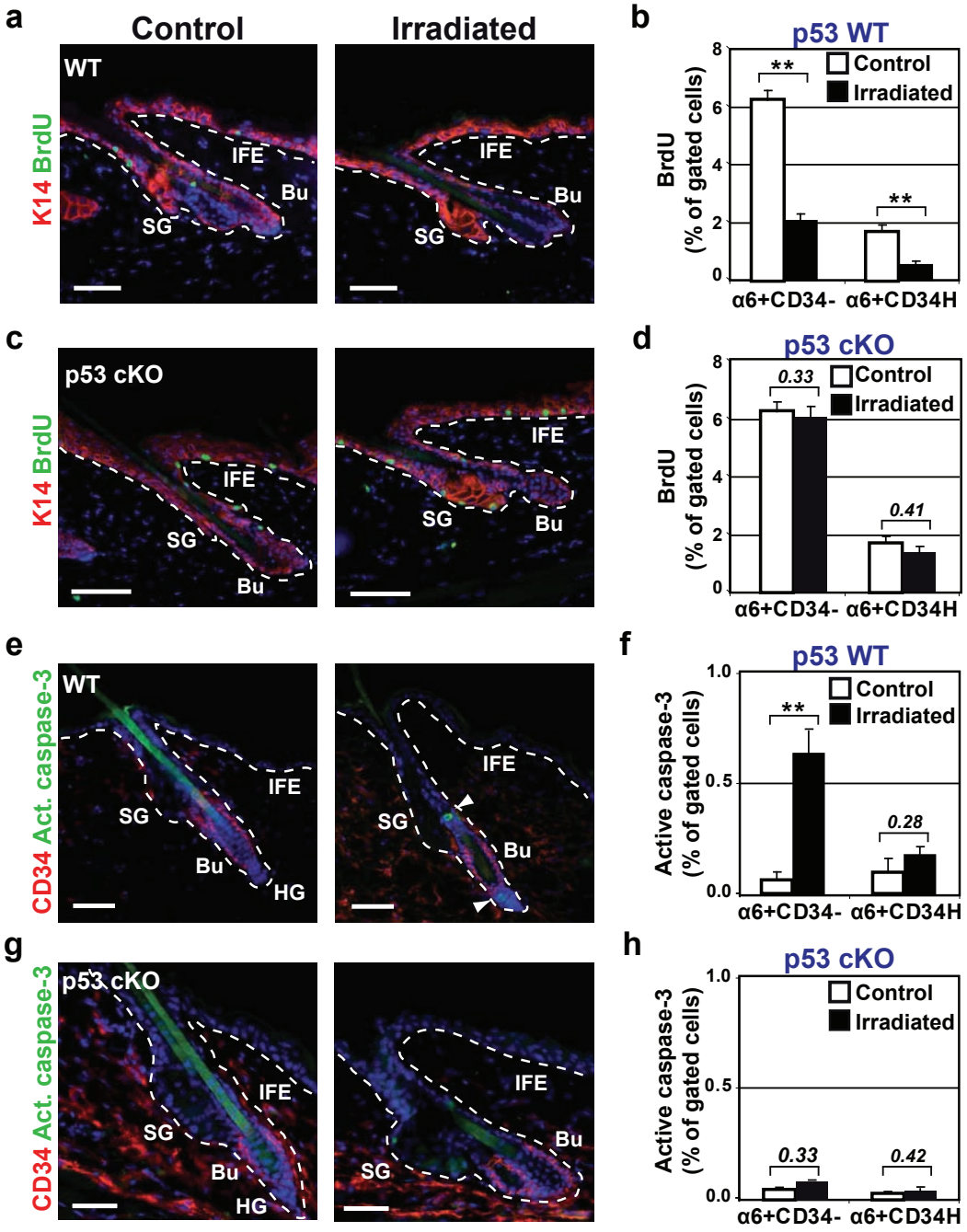

Figure S6 p53 is autonomously required for DNA damage response in the epidermis **(a-d)** Analysis of cell proliferation in epidermal cells of 7-week old p53 positive (p53fl/fl) **(a, b)** and in p53 conditional knockout (p53 cKO) (p53fl/fl-K14CRE) in the epidermis **(c, d)** 24 h after administration of 5 Gy IR by IF **(a, c)** and by FACS analysis **(b, d)** (error bars, s.e.m.; n = 5 mice; 20000 bulge cells/mouse). Note p53 cKO epidermal cells did not undergo cell cycle arrest. **(e - h)** Apoptosis 24 h after administration of 5 Gy IR in p53 wild type **(e, f)** and p53 cKO **(g, h)** epidermal cells, as determined by active caspase-3 immunostaining **(e, g)** and FACS analysis **(f, h)**. Bulge SCs are stained with anti-CD34. Note the lack of active caspase-3 positive cells in irradiated mice of p53 null epidermis, demonstrating that p53 is autonomously required to induce apoptosis in the epidermis following IR (error bars, s.e.m.; n = 8 mice; 20000 bulge cells/mouse). Scale bars represent 50 μm (IFE, interfollicular epidermis; SG, sebaceous gland; Bu, bulge; HG, hair germ).

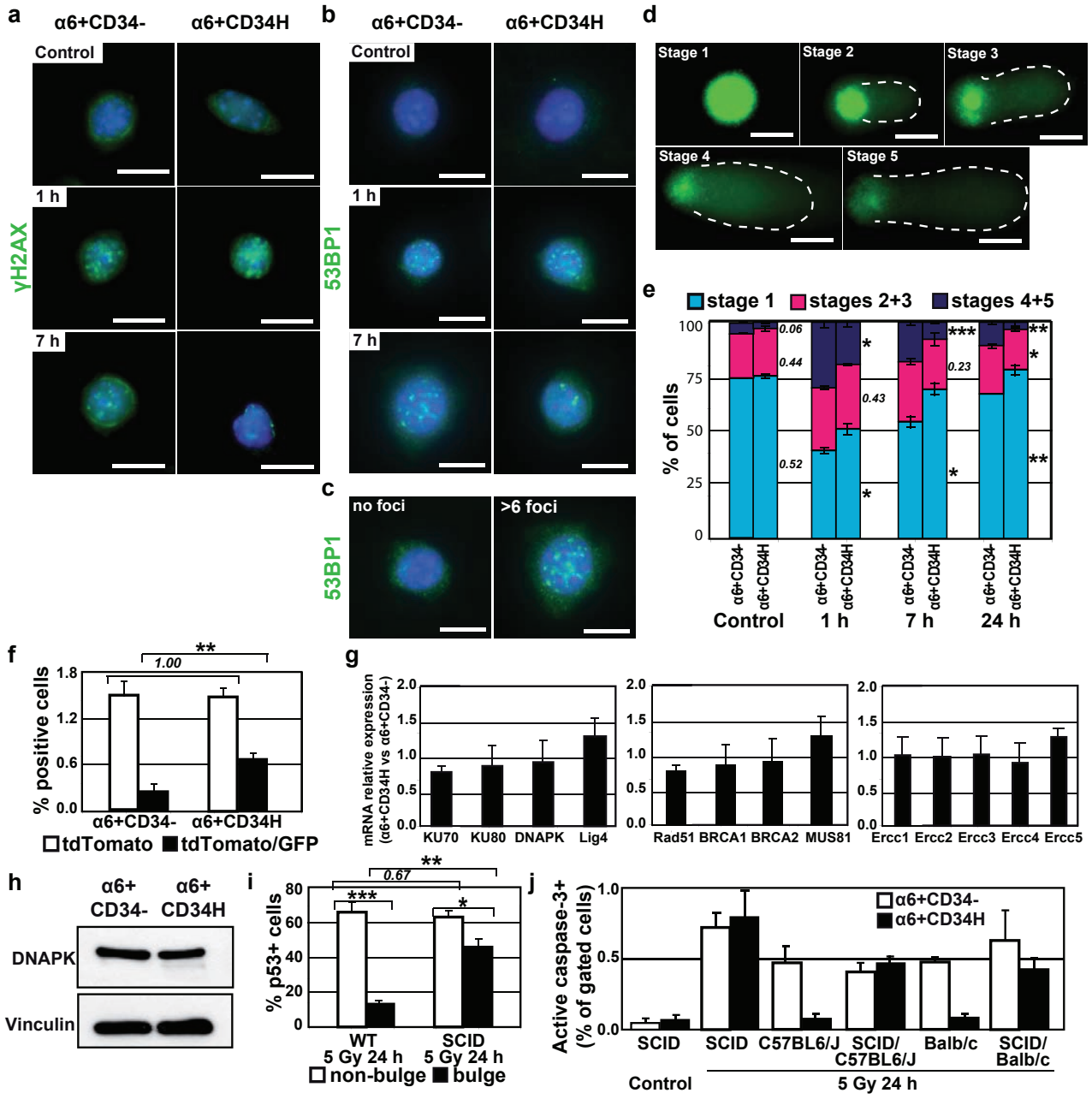

Figure S7 Analysis of DNA damage and repair in epidermal cells **(a)** γH2AX immunostaining of FACS-sorted cells without or after 5 Gy IR. Hoescht dye was used as a nuclear staining. **(b)** IF of 53BP1 expression pattern in FACS-isolated α6+CD34- and α6+CD34H cells. Note the reduction of cells containing multiple 53BP1 nuclear foci (>6 foci/cell) in α6+CD34H cells 7 h after IR. **(c)** Representative images of 53BP1 staining, illustrating the classification used in Fig. 3j. **(d)** Representative images of cells following the Comet assay, illustrating the classification of the different stages. The tails of the comets, corresponding to the fragmented DNA, are surrounded. **(e)** Histogram illustrating the results of neutral comet assay on FACS-isolated cells from mice without and after 5 Gy IR (error bars, s.e.m.; n = 200 cells per group from 3 independent experiments). **(f)** Efficiency of NHEJ in α6+CD34- and α6+CD34H cells measured by the ability to repair linearized GFP reporter plasmids. Co-electroporation with non-digested tdTomato plasmids was used as transfection control (error bars, s.e.m.; n = 8 mice; 20000 bulge cells/mouse). **(g)** Quantitative RT-PCR analysis on FACS-isolated cells of mRNA expression of DNA repair associated genes, showing similar expression of these genes under physiological conditions in the α6+CD34- and α6+CD34H populations. Graphs represent the fold change in gene expression between α6+CD34- and α6+CD34H populations (error bars indicate s.e.m.; n = 5 independent experiments). **(h)** DNAPK expression assessed by western blot analysis using total cellular extracts of FACS-sorted α6+CD34- and α6+CD34H cells. Vinculin was used as loading control. **(i)** Quantification of p53 positive cells on the p53 IHC performed on skin sections of WT and SCID mice 24 h after 5 Gy IR (error bars, s.e.m.; n = 1300 cells per mouse, from 3 WT and 3 SCID mice). **(j)** Quantification by FACS of active Caspase-3 positive cells 24 h after 5 Gy IR in SCID, C57Bl6/J and Balb/c mice, as well as in heterozygous SCID/C57Bl6/J and SCID/Balb/c mice (error bars, s.e.m.; n = 5 mice; 20000 bulge cells/mouse). Scale bars represent 10 μm.

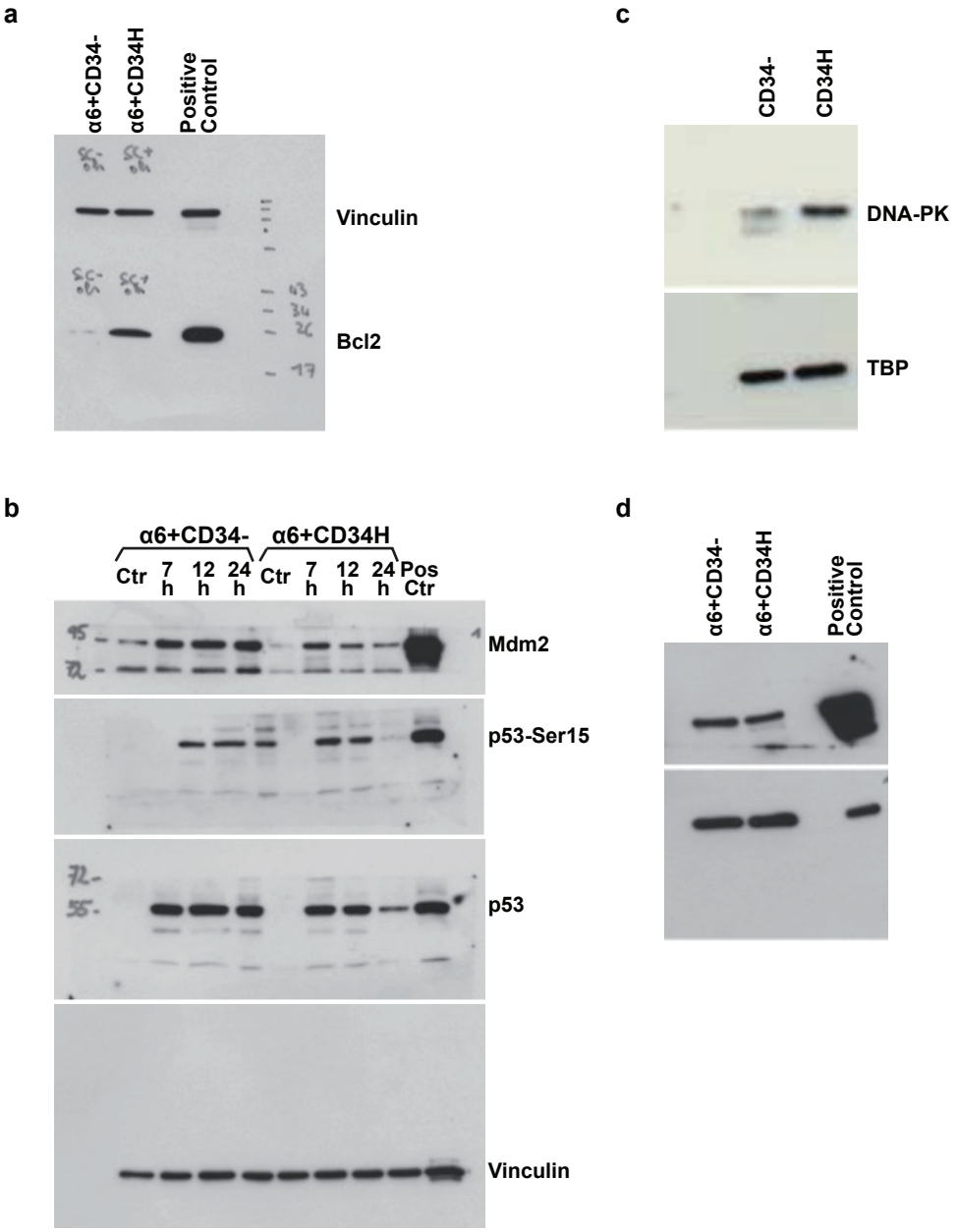

Figure S8 Full length scans of western blots shown in figures 5b **(a)**, 6c **(b)**, 8c **(c)** and supplementary Fig. S12c **(d)**.